


Post-caldera Volcanism at the Heise Volcanic Field: Implications for Petrogenetic Models

Journal Article

Author(s):

Ellis, Ben S.; [Szymanowski, Dawid](#) ; Wotzlav, Jörn-Frederik; Schmitt, Axel K.; Bindeman, Ilya N.; Troch, Juliana; Harris, Chris; Bachmann, Olivier; Guillong, Marcel

Publication date:

2017-01

Permanent link:

<https://doi.org/10.3929/ethz-b-000236705>

Rights / license:

[In Copyright - Non-Commercial Use Permitted](#)

Originally published in:

Journal of Petrology 58(1), <https://doi.org/10.1093/petrology/egx007>

Funding acknowledgement:

146268 - Towards a quantitative understanding of caldera-forming events (SNF)

155923 - Taking apart a 'super' eruption: the Kneeling Nun Tuff, New Mexico (SNF)

Post-caldera Volcanism at the Heise Volcanic Field: Implications for Petrogenetic Models

B. S. Ellis^{1*}, D. Szymanowski¹, J. F. Wotzlaw¹, A. K. Schmitt²,
I. N. Bindeman³, J. Troch¹, C. Harris⁴, O. Bachmann¹ and M. Guillong¹

¹Institut für Geochemie und Petrologie, ETH Zurich, NW Clausiusstrasse 25, 8092 Zurich, Switzerland; ²Institut für Geowissenschaften, University of Heidelberg, Im Neuenheimer Feld 236, 69120 Heidelberg, Germany; ³Department of Geological Sciences, 1272, University of Oregon, Eugene, OR 97403-1272, USA; ⁴Department of Geological Sciences, University Avenue, Upper Campus, University of Cape Town, Rondebosch 7701, South Africa

*Corresponding author. Telephone: +41 44 632 99 73. E-mail: ben.ellis@erdw.ethz.ch

Received March 8, 2016; Accepted January 30, 2017

ABSTRACT

The Heise volcanic field is the second youngest caldera complex of the Yellowstone–Snake River Plain province (USA) and represents a polycyclic caldera system with rhyolitic volcanism extending over more than 2 Myr. The products of the Heise volcanic field include four regionally extensive ignimbrites, including the Blacktail Creek and Kilgore tuffs, which both have volumes estimated at >1000 km³, separated by sequences of smaller volume tuffs, lavas and sedimentary deposits. Rhyolites from the Heise volcanic field are both normal- $\delta^{18}\text{O}$ and low- $\delta^{18}\text{O}$, making it a key locality for investigating rhyolite petrogenesis. However, the occurrence of abundant young basaltic lava has limited our ability to fully characterise this volcanic centre, particularly in terms of post-caldera volcanism. Here we describe rhyolitic samples from both a >700 m thick section of drillcore within the Snake River Plain and the exposed outflow stratigraphy on the margins of the plain. Based on a combination of bulk-rock and mineral geochemical, isotopic, and geochronological evidence, we conclude that the rhyolites from the drillcore are not exposed at the surface, nor are the surficial rhyolites found in the drillcore. High-precision isotope dilution thermal ionisation mass spectrometry U-Pb geochronology dates the rhyolite at the base of the drillcore to 4.0248 ± 0.0011 Ma, ~ 0.4 Myr younger than the youngest caldera-forming ignimbrite at Heise, the 4.48 Ma Kilgore Tuff, whereas U-Pb secondary ionisation mass spectrometry dates the uppermost portion of rhyolite in the drillcore to 3.86 ± 0.19 Ma. The combined geochemistry and stratigraphic relations suggest that the drillcore penetrates the intracaldera stratigraphy. The intracaldera rhyolites are compositionally and mineralogically similar to the outflow stratigraphy with high-temperature magmas (>800°C) persisting for the full >3 Myr history of the Heise centre. The $\delta^{18}\text{O}$ values of pyroxene, sanidine, and quartz from the unaltered drillcore samples are consistent with high-temperature equilibrium and return magma $\delta^{18}\text{O}$ values that are low (4.1–6.0‰ based on $\Delta^{18}\text{O}$ melt–sanidine of 0.6‰) but somewhat higher than the value for the preceding Kilgore Tuff magma of 3.3‰. Buried deep within the drillcore are also hydrothermally altered rhyolites with bulk $\delta^{18}\text{O}$ ranging from –3.5‰ to +1.0‰ (SMOW) with complex X-ray diffraction spectra revealing the presence of epidote, quartz and chlorite. These altered samples are, however, not markedly different in bulk major or trace elemental geochemistry from the unaltered Heise rhyolites. Rhyolite-MELTS models using these hydrothermally altered samples as potential assimilants can reproduce the compositions, mineralogy, and crystallinity of the low- $\delta^{18}\text{O}$ Kilgore Tuff with 40–50% assimilation while also satisfying the mass balance constrained on the basis of $\delta^{18}\text{O}$. These results support a cannibalisation model for Heise volcanism while highlighting that the lowest $\delta^{18}\text{O}$ rhyolites may require large amounts of extremely ^{18}O -depleted hydrothermally altered material available for assimilation.

Key words: cannibalisation; Heise volcanic field; low- $\delta^{18}\text{O}$; rhyolite; Snake River Plain

INTRODUCTION

The generation and storage of large volumes of crystal-poor silicic magma that are commonly erupted from caldera settings remain topics of some debate. In terms of the pre-eruptive storage of silicic magmas, the ability to geochemically interrogate the erupted products in greater detail is leading to an increasing realisation that the pre-eruptive magma storage may take place in discrete batches (e.g. Shane *et al.*, 2007; Ellis *et al.*, 2010; Cooper *et al.*, 2012; Cashman & Giordano, 2014; Wotzlaw *et al.*, 2014, 2015) as well as in large, single magmatic reservoirs (e.g. Bachmann & Bergantz, 2003). How this eruptible magma is ultimately generated remains controversial and despite, or indeed perhaps because of, decades of research, no consensus exists. The debate may be simplified into models that favour fractional crystallisation with some assimilation as the dominant mechanism in rhyolite generation (e.g. Bachmann & Bergantz, 2004; Hildreth, 2004) and those that involve high degrees of crustal melting (e.g. Riley *et al.*, 2001; Wiesmaier *et al.*, 2012; Bindeman & Simakin, 2014). In nature, it is likely that both processes play a role (e.g. assimilation–fractional crystallisation; DePaolo, 1981; Bohron & Spera, 2001); however, the relative dominance of the end-members has important implications for aspects such as magma residence in the upper crust (Coleman *et al.*, 2004; Gelman *et al.*, 2013), timescales of magma generation (Miller & Wooden, 2004; Wotzlaw *et al.*, 2014) and the detectability through geophysical methods of magma accumulations capable of generating voluminous explosive eruptions.

The lack of consensus suggests that both models have limitations. Fractional crystallisation-dominated models have to explain the lack of intermediate compositions in the commonly occurring compositionally bimodal volcanic provinces (e.g. Chayes, 1963; Brophy, 1991; Szymanowski *et al.*, 2015) and the initial volumes required to generate thousands of cubic kilometres of silicic magma via distillation processes. Models favouring crustal melting have to overcome the onerous thermal requirements for melting most crustal lithologies, particularly in the cold upper crust (Annen & Sparks, 2002; Dufek & Bergantz, 2005; Karakas & Dufek, 2015). Isotope geochemistry (Sr, Nd, O, etc.) often requires tens of per cent of a crustal component to be present in silicic magmas (Nash *et al.*, 2006; McCurry & Rodgers, 2009). Oxygen, as a major element in rocks, magmas and fluids, plays an important time (age)-independent tool in defining mass-balance constraints; thus a cornerstone of the crustal melting hypothesis is found in the occurrence of low- $\delta^{18}\text{O}$ magmas requiring a large component of shallow crustal material, in which meteoric water can imprint a low- $\delta^{18}\text{O}$ signature on rocks at large water/rock ratios. Typically, these signatures in $\delta^{18}\text{O}$ are interpreted as being inherited from hydrothermally altered precursors (Taylor, 1968, 1977; Friedman *et al.*, 1974; Bindeman *et al.*, 2001, 2007; Donoghue *et al.*,

2010; Boroughs *et al.*, 2012). However, the lack of phase diagrams for such altered rocks or a detailed appreciation of the mechanisms of melting and assimilation limits our understanding of these processes.

Given this continuing debate, the Yellowstone–Snake River Plain volcanic province (Fig. 1) represents an ideal study location, because rhyolites from the same volcanic centre show characteristics of both fractionation-dominated and crustal melting-dominated parentage. An understanding of magma generation processes within this hotspot-related volcanic province is crucially dependent on detailed studies of the temporal variations in chemistry over the lifetime of the system as a whole. Here we investigate the rhyolites erupted from its second youngest eruptive centre, the Heise volcanic field (Idaho, USA), which are preserved both in outflow stratigraphy and within a drillcore from the centre of the Snake River Plain, to consider how rhyolite generation may occur.

Geological background

The Columbia River–Yellowstone volcanism represents the youngest large igneous province on Earth. Beginning c. 16.5 Ma, the inland north-west of North America was inundated by the voluminous eruptions of the Columbia River Basalt Group (Camp & Ross, 2004; Hooper *et al.*, 2007; Wolff *et al.*, 2008) with approximately simultaneous silicic activity across a broad swath of northern Nevada and eastern Oregon (Brueseke *et al.*, 2008; Coble & Mahood, 2012; Colon *et al.*, 2015). This volcanism is most commonly interpreted as resulting from the Yellowstone hotspot (Geist & Richards, 1993; Yuan & Dueker, 2005). In this work, we use the term hotspot descriptively rather than to invoke any genetic meaning about necessary depth of origin.

Starting at c. 14.5 Ma, the silicic volcanism became focused onto the track of the central Snake River Plain (Pierce & Morgan, 1992; Bonnicksen *et al.*, 2008) with a broadly time-transgressive pattern of activity currently displayed at the Yellowstone Plateau volcanic field (Christiansen, 2001; Fig. 1). The earliest rhyolites in the JP desert (~14–82 Ma) mark this transition (Colon *et al.*, 2015). Compositionally, the Columbia River–Yellowstone province is bimodal, with basalt and rhyolite dominating and volumetrically limited proportions of intermediate rocks (Christiansen & McCurry, 2008). Rhyolitic volcanism is represented by voluminous ignimbrites and extensive lavas commonly proposed to have issued from a number of ‘eruptive centres’, often based on comparison with volcanism at Yellowstone; however, no indisputable evidence for the existence of calderas is known within the central Snake River Plain despite the large volumes of single ignimbrites (Bonnicksen *et al.*, 2008; Branney *et al.*, 2008).

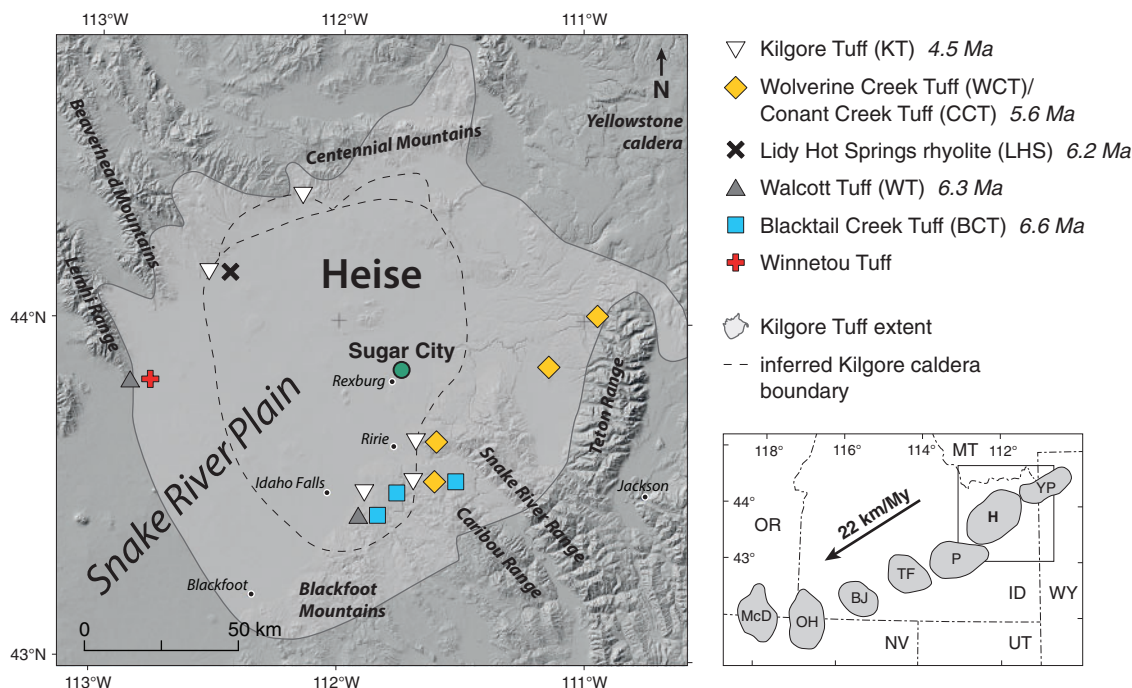


Fig. 1. Map of the Heise eruptive centre in the eastern Snake River Plain showing the locations of the samples collected for this study (each symbol represents a single eruptive unit). The green circle marks the location of the Sugar City drill site. The extent of the Kilgore Tuff ignimbrite sheet, the inferred boundaries of the associated caldera, and the eruption ages are reproduced from Morgan & McIntosh (2005). Index map shows location of the Heise eruptive centre on the Yellowstone hotspot track with successive inferred eruptive centres: McD, McDermitt; OH, Owyhee–Humboldt; BJ, Bruneau–Jarbridge; TF, Twin Falls; P, Picabo; H, Heise; YP, Yellowstone Plateau. The arrow represents the direction and velocity of the North American plate (after Nash *et al.*, 2006).

The Heise eruptive centre

The Heise eruptive centre, located in the eastern Snake River Plain (Fig. 1), provides a record of silicic volcanism from the Yellowstone hotspot between ~6.6 and 4.0 Ma (Morgan & McIntosh, 2005; Watts *et al.*, 2011). To the north and south of the plain a series of ignimbrites is preserved, yet within the plain itself the rhyolitic ignimbrites are generally covered by younger basaltic lavas. The eruptive centre has previously been defined as containing a series of ignimbrites beginning with the Blacktail Creek Tuff (6.62 Ma) and ending with the Kilgore Tuff (4.45 Ma) with minor rhyolitic lavas extending to ~4.0–3.8 Ma (Morgan & McIntosh, 2005; Bindeman *et al.*, 2007; Watts *et al.*, 2011). The units underlying the Blacktail Creek Tuff are poorly known, with many of them described only with reconnaissance-scale geochemical work (e.g. Drew *et al.*, 2013). As with many locations along the central Snake River Plain (CSRP), the division between units inferred to be from a specific eruptive centre, in this case the older Picabo centre (Drew *et al.*, 2013), or the Heise eruptive centre (e.g. Watts *et al.*, 2011), may be entirely arbitrary. This study defines the base of the Heise volcanic package by the occurrence of the newly described Winnetou Tuff, which differs geochemically and petrologically from the overlying Heise succession.

Separating the Blacktail Creek Tuff and Kilgore Tuff are a variety of ignimbrites, smaller volume pyroclastic

deposits, rare lavas including the Lidy Hot Springs lava, and sedimentary intervals (Morgan *et al.*, 1984; Morgan & McIntosh, 2005; Watts *et al.*, 2011). The main ignimbrites within this sequence are the Walcott Tuff (6.27 Ma), the Wolverine Creek Tuff (5.59 Ma), and the Conant Creek Tuff (5.51 Ma; Morgan & McIntosh, 2005). Generally, the deposits are separated by significant time breaks (hundreds of thousands of years), but the Conant Creek and Wolverine Creek tuffs have eruption ages that overlap according to the $^{40}\text{Ar}/^{39}\text{Ar}$ geochronology of Morgan & McIntosh (2005). These two relatively large pyroclastic deposits, although differing in field appearance, are near-identical in mineral, glass and bulk-rock geochemistry as well as zircon crystallisation ages (Szymanowski *et al.*, 2015, 2016) and thus are here considered eruptions from the same magma reservoir.

Despite considerable study, the sources of the ignimbrites thought to be produced from the Heise volcanic centre (schematically shown in Fig. 1) remain enigmatic, a problem common throughout the Snake River Plain as a whole owing to Basin and Range extension and later basalt effusion. Only the Blacktail Creek Tuff shows a dramatic thickness variation (from 10 to >100 m over a lateral distance of a few hundred metres) inferred to represent the effect of crossing a caldera boundary (Morgan & McIntosh, 2005; Engleman *et al.*, 2013). However, even in this case, the caldera boundary

is cryptic, in that no classic features of caldera margins such as breccias, hydrothermal alteration, or buttress-style contacts are present (see Lipman, 1997, for a review). Field evidence for other calderas is equivocal or absent. Importantly, the volume estimates previously provided for the ignimbrites of the Heise eruptive centre include a significant thickening (to >1 km) thought to occur within the calderas (Morgan & McIntosh, 2005); the thickest ignimbrites we are aware of are of the order of a few hundred metres. Clearly the poorly known location, geometry, and structure of such calderas are a first-order source of uncertainty in understanding the Heise volcanic system.

The Sugar City drillcore

Originally drilled in 1978, the exploration drillcore in Sugar City, Idaho (Fig. 1), hereafter referred to as the Sugar City core or just the drillcore, penetrates to a depth of ~700 m. Since the original descriptions by Embree *et al.* (1978), the core has remained largely unstudied. The upper 140 m are dominated by young basaltic lavas, similar to the surficial geology of the Pleistocene Snake River Plain. Intercalated within this package is a ~12 m thick deposit of Huckleberry Ridge Tuff pinning the age of that horizon to ~2.1 Ma (Singer *et al.*, 2014; Wotzlaw *et al.*, 2015). Our study focuses on the lower portion of the drillcore between 140 and 700 m (Fig. 2) in an attempt to link these deposits to those of the surficial stratigraphy on the margins of the Snake River Plain. We mainly focus on two lithologies occurring in the drillcore. The first of these is vitrophyric layers, as these record the quenching of hot, rhyolitic melt against a cool medium, typically the air or the ground, and commonly represent the uppermost and lowermost portions of a deposit (e.g. Branney *et al.*, 2008). The second focus is the visibly altered lithologies that occur towards the base of the drillcore, which may represent suitable source materials for the low- $\delta^{18}\text{O}$ rhyolitic magmas.

METHODS

Samples of units in this study were collected from locations around the eastern Snake River Plain (Fig. 1; exact locations are detailed in the Supplementary Data, available for downloading at <http://www.petrology.oxfordjournals.org>). All samples were crushed and minerals and glass were separated by a combination of magnetic separation, heavy liquids (sodium polytungstate), and handpicking under a binocular microscope. Grain separates for mineral chemistry were mounted in epoxy, polished and mapped using transmitted light and back-scattered electron microscopy. For crystal-rich varieties of the Blacktail Creek and Kilgore tuffs and drillcore rhyolites, thin sections were prepared to assess textural relationships. A complete dataset is given in the Supplementary Data, including data for reference materials.

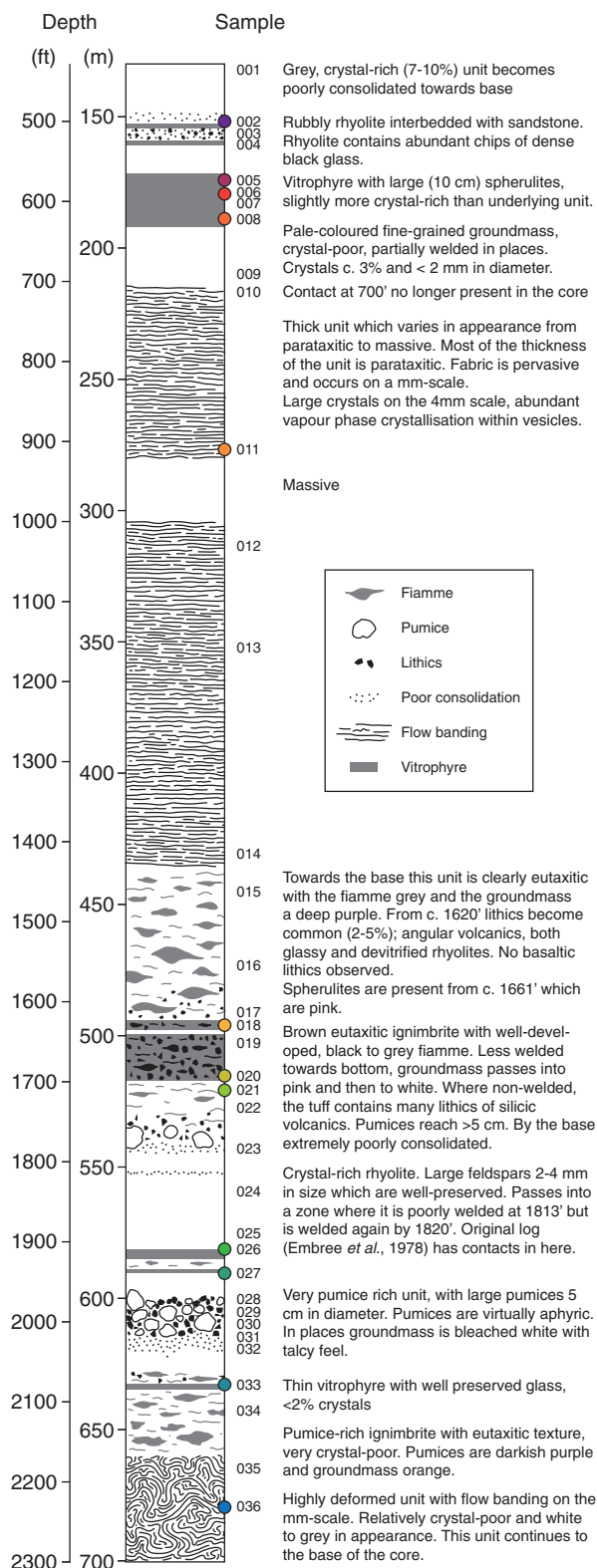


Fig. 2. Stratigraphic log of the lower portion of the Sugar City drillcore with sample locations marked.

Whole-rock major and trace element X-ray fluorescence (XRF) analyses were performed at ETH Zurich using a 2.4 kW PANalytical Axios wavelength-dispersive X-ray spectrometer. Aliquots of rocks were ground to

fine powder (~1.5 g), heated to 950°C for 2 h and reweighed when cool to determine the loss on ignition (LOI). The desiccated powders were then fused with lithium tetraborate ($\text{Li}_2\text{B}_4\text{O}_7$) flux (1:5 mixture) in Pt–Au crucibles and quenched to produce round beads. For X-ray diffraction (XRD) analysis, sample powders were homogenised and randomly oriented powders were prepared via front-loading by sprinkling onto standard sample holders and flattening of the powder by vertical hitting with a razor blade. XRD analysis was performed on a Bruker D8advance X-ray diffractometer equipped with a LynxEye-detector, in the scan range 4.5–90° (2 θ). Step size was set to 0.02° with a measuring time of 2.5 s per step. All samples were measured in rotation mode to reduce preferred orientation effects.

Major element abundances in feldspar, pyroxene and glass were determined with a JEOL JXA-8900R electron microprobe at the University of Kiel or a JEOL JXA-8200 at ETH Zurich using wavelength-dispersive spectrometry mode with a 15 kV accelerating voltage and 15 nA beam current for pyroxenes and feldspars and a reduced current of 12 nA for glasses. A fully focused beam was used for pyroxene, and defocused beams of 20 μm diameter for the glasses and 5 μm for feldspars were selected to minimise effects related to element mobility (e.g. Na, K). To ensure instrument stability throughout the measurement, secondary standards were used (Jarosewich *et al.*, 1980): Kakanui augite NMNH 122142 for pyroxenes, Lake County labradorite USHM 115900 for feldspars and Yellowstone rhyolitic glass VG-568 (NMNH 72854) for glass.

Trace element concentrations in plagioclase, sanidine, pyroxene, and glass, as well as Pb isotopes in sanidine and glass, were determined via laser ablation inductively coupled plasma mass spectrometry (LA-ICP-MS) using a 193 nm Resonetics ArF excimer laser coupled to a Thermo Element XR ICP-MS system at the Institute of Geochemistry and Petrology, ETH Zurich. Additional trace element determinations in feldspars were made with a 193 nm excimer ArF laser attached to a PerkinElmer ELAN 6100 ICP-MS system, also at ETH Zurich. Spot sizes were adjusted depending on grain size and set at 43 or 67 μm for every run with the output energy of the laser maintained at ~3.5 J cm^{-2} . For all trace element determinations, a set of two NIST612 and additional standard glasses GSD-1 G and BCR-2 G (one each) were measured after every 25 unknowns to monitor for drift. Raw data were reduced using the MATLAB-based program SILLS (Guillong *et al.*, 2008); all trace element determinations are considered to have precision better than 5% based on homogeneous standard reproducibility. Measured $^{208}\text{Pb}/^{206}\text{Pb}$ and $^{207}\text{Pb}/^{206}\text{Pb}$ isotopic ratios in sanidine and glass were normalised to the NIST612 silicate glass standard, with reference values of 2.1647 and 0.9073 respectively (Jochum & Stoll, 2008). Standard isotope ratios were reproducible typically within 0.3% (2SD).

Zircon U–Pb ages were determined by secondary ionisation mass spectrometry (SIMS) using the

CAMECA ims 1270 ion microprobe at the University of California Los Angeles (UCLA). Analytical procedures (including a common Pb correction using measured ^{207}Pb , and a correction of initial ^{230}Th disequilibrium) follow those described by Schmitt *et al.* (2003). Common $^{207}\text{Pb}/^{206}\text{Pb} = 0.8283$, corresponding to anthropogenic surficial contamination of the ion probe mounts, and a $D_{\text{Th}}/D_{\text{U}}$ zircon–melt partition coefficient ratio of 0.2 was used, which agrees well with average zircon Th/U = 0.8 and whole-rock Th/U = 4.5 (see below). All ages are relative to zircon reference AS3 with a $^{206}\text{Pb}/^{238}\text{U}$ age of 1099 Ma (Paces & Miller, 1993); the uncertainty of the calibration translates into a relative error for the $^{206}\text{Pb}/^{238}\text{U}$ ages of 1.7% (1SD; $n = 33$). Uranium concentrations are relative to zircon reference 91500 with U = 81 ppm (Liu *et al.*, 2010). Ion microprobe Th/U was calibrated using radiogenic $^{208}\text{Pb}/^{206}\text{Pb}$ for AS3.

Selected zircons from the basal unit 14 036 (Fig. 2) were dated by chemical abrasion isotope dilution thermal ionisation mass spectrometry (CA-ID-TIMS) at ETH Zurich. All selected crystals were placed in quartz crucibles and annealed for 48 h at 900°C in a muffle furnace. Single crystals were then loaded with a microdrop of 7 N HNO_3 and 70 μl HF in 200 μl Savillex microcapsules for chemical abrasion (Mattinson, 2005). The loaded microcapsules were assembled in a Teflon liner filled with 7 ml HF + trace HNO_3 that was placed in a Parr pressure vessel; zircons were partially dissolved for 12 h at 180°C. Remaining crystals and crystal fragments were transferred into 3 ml Savillex beakers, fluxed in 6N HCl on a hotplate and ultrasonically cleaned in 4N HNO_3 before transferring them back into their pre-cleaned microcapsules with a microdrop of 7N HNO_3 and 70 μl HF. Samples were spiked with 6–8 mg of the EARTHTIME ^{202}Pb – ^{205}Pb – ^{233}U – ^{235}U tracer (Condon *et al.*, 2015; McLean *et al.*, 2015) and zircons were dissolved for ~60 h at 210°C in Parr vessels. After dissolution, samples were dried down and redissolved in 6N HCl at 180°C for ~12 h to convert samples to chlorides. After redissolution, samples were dried down again and taken up in 3N HCl for ion exchange chemistry. Pb and U were separated employing an HCl-based single column chemistry modified from Krogh (1973). U–Pb fractions were loaded together on outgassed Re-filaments and measured sequentially on a Thermo TRITON Plus thermal ionisation mass spectrometer. Pb was measured in dynamic mode on a MasCom secondary electron multiplier and U was measured as UO_2 in static mode on Faraday cups equipped with 10^{11} ohm resistors. Mass fractionation was corrected using the double spike. Pb mass fractionation factors were derived from the measured $^{202}\text{Pb}/^{205}\text{Pb}$ ratio normalised to the true value of 0.99924 (Condon *et al.*, 2015). U isotopic ratios were corrected for isobaric interferences of $^{233}\text{U}^{18}\text{O}^{16}\text{O}$ on $^{235}\text{U}^{16}\text{O}_2$ using an $^{18}\text{O}/^{16}\text{O}$ of 0.00205 ± 0.000025 and for mass fractionation using the measured $^{233}\text{U}/^{235}\text{U}$ ratio relative to the true value of 0.99506 (Condon *et al.*, 2015) and a sample $^{238}\text{U}/^{235}\text{U}$ of 137.818 ± 0.045 (Hiess *et al.*, 2012). All common Pb in

zircon analyses was attributed to laboratory blank and corrected with the average composition of total procedural blank measurements (see Supplementary Data). Data reduction was performed using the Tripoli and U–Pb_Redux software package (Bowring *et al.*, 2011), which uses the data reduction and uncertainty propagation algorithms of McLean *et al.* (2011). U–Pb ratios and dates were calculated relative to a tracer $^{235}\text{U}/^{205}\text{Pb}$ ratio of $100.23 \pm 0.046\%$ (2σ) and using the decay constants of Jaffey *et al.* (1971). The $^{206}\text{Pb}/^{238}\text{U}$ ratios and dates were corrected for initial ^{230}Th disequilibrium using a Th/U of 4.5 ± 0.5 for the magma, based on the bulk-rock trace element analyses. All uncertainties are reported at the 2σ level and ignore systematic uncertainties associated with the tracer calibration and decay constants (Jaffey *et al.*, 1971; McLean *et al.*, 2015).

Oxygen isotope analyses were performed at the University of Oregon stable isotope laboratory, where mineral separates ranging in weight from 0.6 to 2 mg were analysed on a MAT 253 mass spectrometer following methods described by Bindeman (2008). Standards were analysed together with the unknowns during each analytical session with the UOG standard ($\delta^{18}\text{O} = 6.52\text{‰}$) stable throughout the analyses of unknowns. Values are reported in standard per mil notation relative to V-SMOW and uncertainties are $\pm 0.15\text{‰}$ (2SD on standards). Whole-rock powders were analysed using a conventional silicate line at the University of Cape Town, following methods described by Harris & Ashwal (2002). Approximately 10 mg of sample was reacted with ClF_3 , and the liberated O_2 was converted to CO_2 using a hot platinised carbon rod. O-isotope ratios were measured off-line using a Finnigan Delta XP mass spectrometer in dual-inlet mode. All data are reported in δ notation where $\delta^{18}\text{O} = (R_{\text{sample}}/R_{\text{standard}} - 1) \times 1000$ and R is the measured $^{18}\text{O}/^{16}\text{O}$ ratio. Duplicate splits of the internal quartz standard (MQ) were run with each batch of eight samples, and were used to convert the raw data to the SMOW scale using a $\delta^{18}\text{O}$ value of 10.1‰ for MQ. The long-term variability of the quartz standards analysed suggests a 2σ error of 0.16‰ . Yields were measured for all conventional analyses by means of a small-volume cold finger and a pressure transducer during the extraction procedure, and were close to the expected 100% yield based on the weight and composition of the sample.

RESULTS

Petrography

The Heise rhyolites are generally crystal-poor, ranging from the almost aphyric Conant Creek Tuff to the Blacktail Creek Tuff with $\sim 20\%$ crystals. Typically these rhyolites are between 5 and 10% crystalline (point counts for drillcore rhyolites are provided in the Supplementary Data). The mineral assemblage is identical between the outflow rhyolites and the drillcore units, comprising plagioclase \pm sanidine \pm quartz + augite \pm orthopyroxene + Fe–Ti oxides + accessory

zircon and apatite. Pigeonite occurs in trace quantities in some rhyolites, but is a major component of the stratigraphically lowest outflow unit in this study, the informally named Winnetou Tuff (where it occurs together with orthopyroxene). The limited occurrence of hydrous phases in these rhyolites is consistent with the hot, dry nature of rhyolites from the Central Snake River Plain (CSRP) (e.g. Honjo *et al.*, 1992; Bonnicksen *et al.*, 2008). In addition to single crystals, crystal aggregates commonly occur containing plagioclase, pyroxene, Fe–Ti oxides and accessory phases (Watts *et al.*, 2011), similar to crystal aggregates found in units from the CSRP, which have been interpreted as cumulate fragments (Ellis *et al.*, 2014) owing to the disequilibrium between their mineral compositions suggesting crystallisation from a rhyolitic melt and bulk compositions that are significantly less evolved.

Bulk compositions

All samples analysed here are rhyolitic and most are high-silica rhyolites with $>75\text{ wt } \%$ SiO_2 (full data are given in the Supplementary Data). Bulk compositions are similar to those previously reported from both the Heise volcanic field (Watts *et al.*, 2011) and the Yellowstone–Snake River Plain (YSRP) province as a whole (Hildreth *et al.*, 1984; Bonnicksen *et al.*, 2008; Ellis *et al.*, 2010). Multiple analyses of single units reveal that major ignimbrite sheets at Heise are compositionally homogeneous, both laterally between outcrops and vertically within single profiles. The low-volume units of Wolverine Creek Tuff and Conant Creek Tuff show characteristically low Ba contents (~ 500 ppm, also recorded by Morgan, 1992; Watts *et al.*, 2011), with the Wolverine Creek Tuff additionally having elevated Al_2O_3 and MgO abundances, which are the result of it containing cumulate pyroxenes from an intermediate magma (Szymanowski *et al.*, 2015, 2016). The Kilgore Tuff has higher Zr contents (318–410 ppm) than other Heise rhyolites. The rhyolites from the drillcore are compositionally similar to those observed on the surface (with Zr contents between 181 and 260 ppm).

Chondrite-normalised rare earth element (REE) patterns are identical between all samples and also to previously published data from the province, showing the classic ‘seagull’ shape with flat heavy REE (HREE) and a negative Eu anomaly ($\text{Eu}/\text{Eu}^* \sim 0.2\text{--}0.5$). Notably, the less negative Eu anomalies are observed in the more crystal-rich Winnetou and Blacktail Creek Tuff samples. The REE patterns are attributed to the fractionation of plagioclase with minimal involvement of middle REE (MREE)-hosting phases such as titanite or amphibole, consistent with the observed mineralogy (Bachmann & Bergantz, 2008). Such REE patterns are typical for both glasses and bulk-rocks in the crystal-poor rhyolites of the Snake River Plain–Yellowstone province (e.g. Morgan *et al.*, 1984; Ellis *et al.*, 2013).

Glass compositions

Where the ignimbrites are strongly welded, only dense glass is observed, presumably owing to bubble collapse and textural homogenisation during the welding process; however, within the non-welded units (Kilgore Tuff sample BP5-25-12-2, Wolverine Creek Tuff DS13003), multiple morphologies of glass may be discerned that are indistinguishable in their trace element abundances. In the unwelded Kilgore and Wolverine varieties, glass occurs as large, macrovesicular shards (common to the ignimbrites of the central Snake River Plain; e.g. [Branney *et al.*, 2008](#)), microvesicular pumiceous clasts and non-vesicular, dense, black clasts.

All types of analysed glass are rhyolitic with SiO₂ contents of 76–77 wt % (recalculated on an anhydrous basis; see the Supplementary Data), with compositions showing excellent agreement with those previously reported by [Perkins *et al.* \(1995\)](#) and [Perkins & Nash \(2002\)](#) for distant airfall deposits. Compositions of glass from basal and upper vitrophyres are identical, indicating essentially no compositional variation within a deposit. Major element variations between Heise units are slight, except for the Blacktail Creek Tuff, which has distinctly lower Na₂O and higher K₂O contents, and the Walcott Tuff and Lidy Hot Springs rhyolite, with slightly elevated MgO contents. However, trace element concentrations in glasses are more distinctive, allowing for confident unit discrimination based on variations observed in, for example, Ti, Rb, Y, Zr, Nb, Ba, La, Ce and U ([Fig. 3](#)). The majority of samples from the drillcore are compositionally identical, with only sample 14 027 being distinct. Many trace elements from drillcore glasses do not overlap in composition with any of the rhyolites on the surface. However, REE concentrations in glasses from all Heise rhyolites are almost identical [including the pronounced negative Eu anomaly (Eu/Eu* ~ 0.2–0.3); [Fig. 3](#)].

Feldspar compositions

Feldspar constitutes the most abundant mineral phase in all Heise rhyolites, occurring as both plagioclase and sanidine, with the relative abundance of the two minerals varying significantly between units. The two feldspars are equally abundant in the Blacktail Creek Tuff, Conant Creek Tuff and Lidy Hot Springs rhyolite, whereas sanidine is less abundant in the Winnetou Tuff and extremely rare in the Walcott Tuff (1% of total feldspar). In most units feldspars are subhedral to euhedral and range in size up to 1 mm in longest direction (a few millimetres in the Blacktail Creek Tuff). In general, feldspar crystals lack obvious zonation ([Fig. 4a](#) and [b](#)), yet often sanidine-rich units contain complex intergrowths of plagioclase and sanidine, particularly within the cores of the grains, where sanidine mantles a core of plagioclase ([Fig. 4c](#) and [d](#)). In addition to the overgrowth rims, sanidine always occurs as single unzoned phenocrysts ([Fig. 4b](#)). Although mantled feldspars occur in all sanidine-bearing Heise units, this feature is particularly common in the Kilgore Tuff, where it represents ~20% of all feldspar grains.

The feldspars from Heise rhyolites are compositionally variable, with major element compositions spanning the range from plagioclase with An₄₆ to sanidine with Or₇₀ with rare outliers of up to An₆₈ ([Fig. 5](#)). This range of feldspar compositions is in contrast to the rhyolites of the CSR, which contain plagioclase of An_{25–50} and sanidine of Or_{50–62} ([Cathey & Nash, 2004](#); [Ellis *et al.*, 2013](#)). Within single phenocrysts or separate domains within a crystal (i.e. where sanidine overgrows plagioclase), compositional zonation is very limited, typically <5% An core to rim variation. Where anhedral plagioclase cores are mantled by sanidine rims, the range of compositions is indistinguishable from that of the unzoned crystals. The plagioclase range reported here is somewhat larger than that

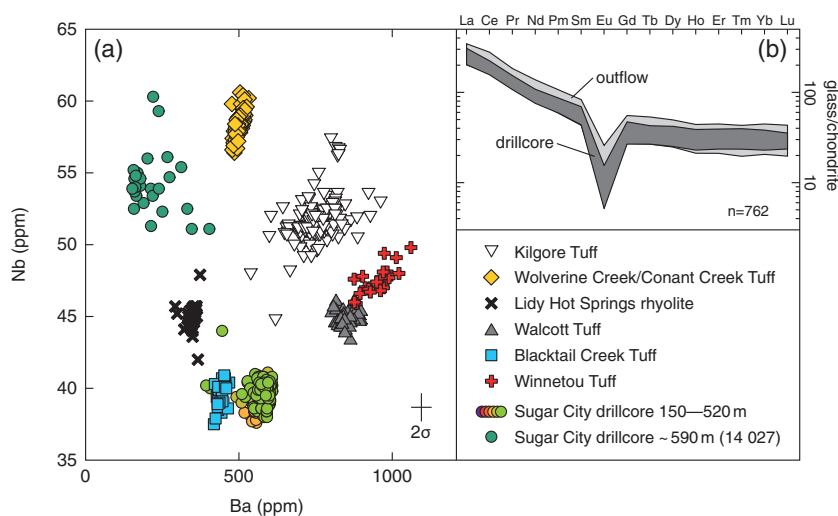


Fig. 3. Trace element compositions of glasses from the Heise rhyolites. (a) Nb–Ba diagram illustrating the utility of glass trace elements in distinguishing the regional eruptive units. (b) A compilation of chondrite-normalised glass rare earth element (REE) patterns for both outflow and drillcore rhyolite samples showing a typical ‘seagull’-shaped REE pattern, which also characterises whole-rock compositions in these highly evolved, crystal-poor rhyolites. Symbols for drillcore samples as in [Fig. 2](#).

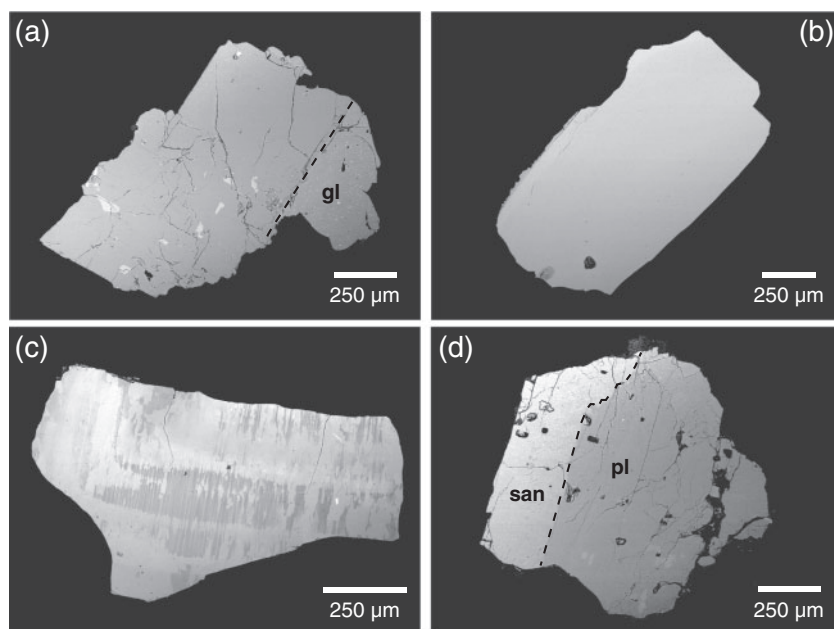


Fig. 4. Backscattered electron (BSE) images of feldspars from the Heise rhyolites. (a) Typical compositionally homogeneous plagioclase with adhering glass (14 005). (b) Typical homogeneous sanidine from the Wolverine Creek Tuff. (c, d) Examples of complex overgrowth textures in feldspar. (c) Skeletal remnants of plagioclase (dark) surrounded by (bright) sanidine from the Wolverine Creek Tuff; (d) plagioclase core mantled by a sanidine rim in the Kilgore Tuff.

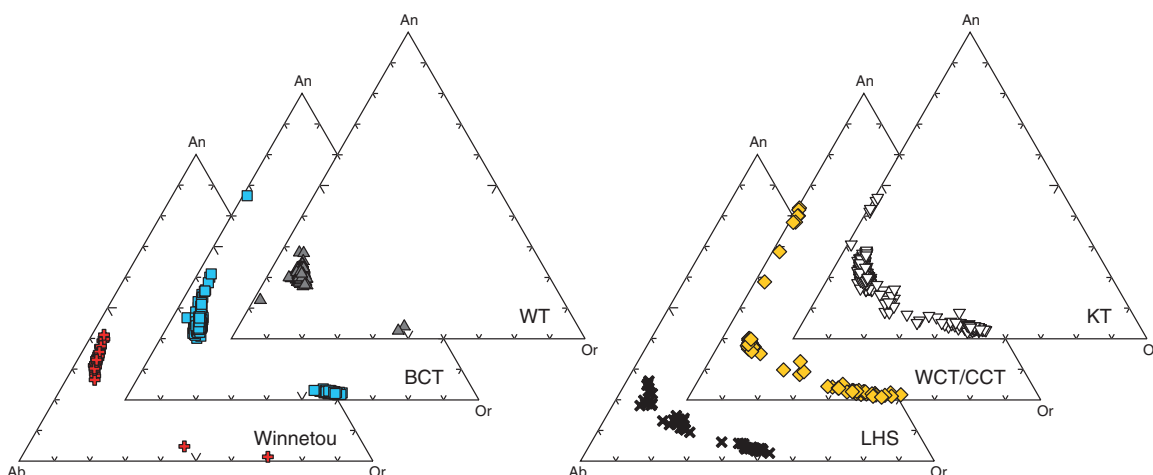


Fig. 5. Major element compositions of feldspars from the regional Heise ignimbrites. BCT, Blacktail Creek Tuff; WT, Walcott Tuff; LHS, Lidy Hot Springs rhyolite; WCT/CCT, Wolverine Creek Tuff–Conant Creek Tuff; KT, Kilgore Tuff. Symbols as in Fig. 3.

observed in previous studies (Henshaw, 2002; Watts *et al.*, 2011), which might be expected given the much larger number of analyses. Our results show that inter-ignimbrite variation in feldspar major elements is limited, rendering attempts to use feldspar major element composition as a discrimination tool problematic (cf. Anders *et al.*, 2014).

Much more revealing is the trace elemental composition of Heise plagioclase. Trace elements, particularly Ba, Sr, Ti, Eu, Ce and La, are distinct between plagioclase from different units and so may be used as a ‘fingerprint’ of a distinct magma (Fig. 6). In general, the large-volume units (Blacktail, Walcott, Kilgore) have similar trace element characteristics (yet without a clear

temporal trend; Fig. 6), whereas less voluminous ignimbrites and lavas bear distinct signatures outside the main compositional field. The oldest tuff sampled, the Winnetou Tuff, has higher Ti than the younger rhyolites. As noted by Szymanowski *et al.* (2015), the Conant Creek and Wolverine Creek tuffs have identical plagioclase compositions (Fig. 6). Plagioclase grains from the majority of drillcore samples have similar trace element abundances, which differ from those in the surficial rhyolites, excepting slight overlap with the Blacktail Creek Tuff and Wolverine–Conant Creek Tuff. The lowest sample from the core, 14 036, is compositionally distinct from both the outflow rhyolites and the other drillcore samples (Fig. 6).

Pyroxene compositions

The majority of the rhyolites from the Heise eruptive centre contain augite and orthopyroxene, in contrast to the augite and pigeonite assemblage that typifies rhyolites of the CSRP (Watts *et al.*, 2011; Ellis *et al.*, 2013). Furthermore, the Heise rhyolites mostly contain single compositional populations of augite and orthopyroxene rather than the multiple compositional populations of augite and orthopyroxene that are common among the

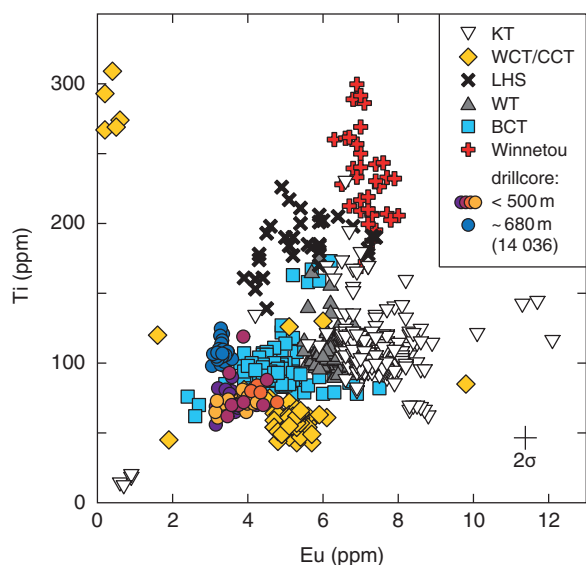


Fig. 6. Trace element compositions of plagioclase from the Heise rhyolites illustrating the compositional differences between the units. The exotic WCT/CCT plagioclases plotting at high Ti, low Eu represent the primitive population described by Szymanowski *et al.* (2015). Symbol colours for drillcore samples are identical to those in Fig. 2.

CSRP rhyolites (e.g. Cathey & Nash, 2004). Virtually all pyroxenes yet reported from the Snake River Plain are compositionally homogeneous (Figs 7 and 8), with the cumulate pyroxenes observed in the Wolverine Creek Tuff being the only known exception (Szymanowski *et al.*, 2015). In contrast to the feldspars of the Snake River Plain, the major element compositions of pyroxenes have been shown to be reliable in discriminating between magma batches (e.g. Honjo *et al.*, 1992; Cathey & Nash, 2004; Ellis & Wolff, 2012). Pyroxene compositions in the major regional ignimbrites from the Heise field agree well with the limited previously published data for these units (e.g. Henshaw, 2002; Watts *et al.*, 2011; Bolte *et al.*, 2015). Interestingly, the stratigraphically lowest rhyolite we sampled, the Winnetou Tuff, contains both pigeonite and orthopyroxene, suggesting a greater affinity with the CSRP system than with the Heise system (Fig. 8).

Pyroxenes from the Sugar City core are also augite and orthopyroxene and have compositions that may be separated into distinct groups of samples. The first group contains samples 14 002–14 011 and the second group contains 14 026 and 027. The lowest samples from the core (14 033 and 036, Fig. 8) are distinct from the overlying samples, and, although they have overlapping augite compositions, sample 14 036 appears to contain little or no orthopyroxene whereas sample 14 033 contains both in roughly equal proportions. A notable feature of the drillcore pyroxene data is the extremely limited occurrence of compositions that overlap with those of Kilgore Tuff pyroxenes (shown as a shaded field in Fig. 8b).

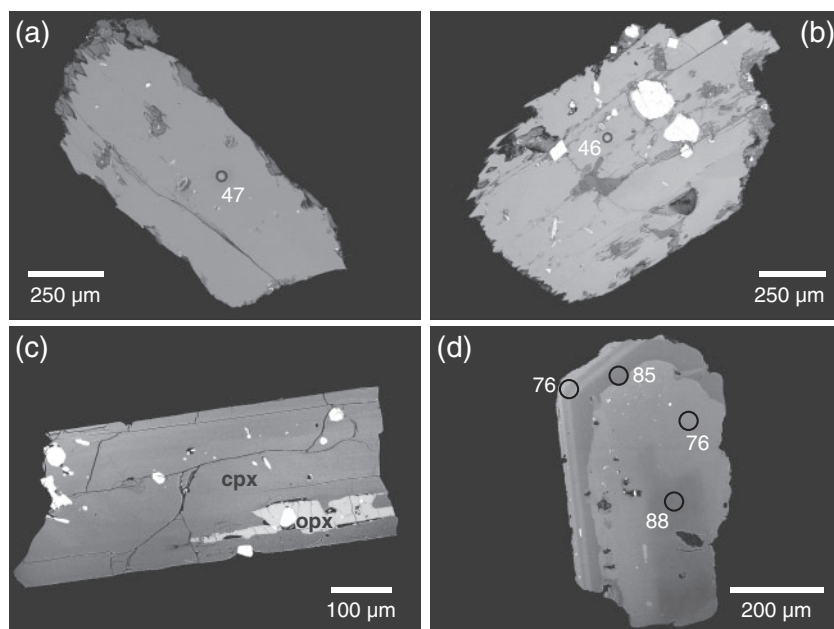


Fig. 7. Backscattered electron (BSE) images of clinopyroxenes from the Heise rhyolites marked with the measured Mg# [Mg/(Mg + Fe)]. (a–c) Typical internally homogeneous crystals of clinopyroxene (a, b, CCT; c, 14 005) with inclusions of Fe–Ti oxides (b) and orthopyroxene (c). (d) Zoned clinopyroxene present only in the Wolverine Creek Tuff (Szymanowski *et al.*, 2015).

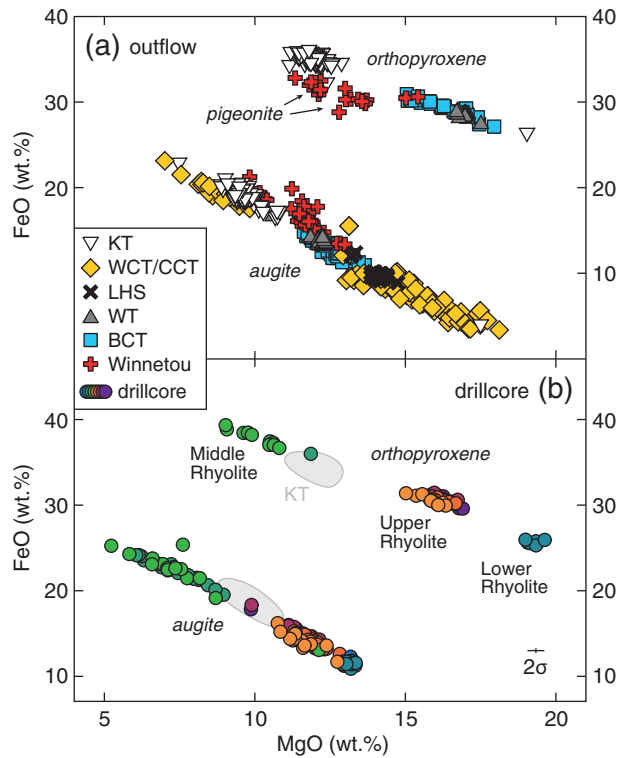


Fig. 8. Compositions of pyroxenes from all major outflow rhyolites exposed on the surface (a) and within the Sugar City drillcore (b). The occurrence of augite, pigeonite and rare orthopyroxene in the Winnetou unit should be noted. For comparison, the range of Kilgore Tuff pyroxene compositions is shown in (b) with grey shading. Symbol colours for drillcore samples are identical to those in Fig. 2; the designations of geochemically defined units within the drillcore are partly based on pyroxene compositions (see Discussion).

Oxygen isotopes

Rhyolites of the Yellowstone–Snake River Plain province represent the largest known suite of low- $\delta^{18}\text{O}$ magmas on Earth. In the CSRP, the rhyolites are almost exclusively low- $\delta^{18}\text{O}$, reaching values as low as -1% (Boroughs *et al.*, 2012; Colon *et al.*, 2015), whereas in the Picabo, Heise, and Yellowstone centres, trends from normal- to low- $\delta^{18}\text{O}$ rhyolites occur (Hildreth *et al.*, 1991; Bindeman *et al.*, 2007; Watts *et al.*, 2011; Drew *et al.* 2013).

Mineral separates

We re-analysed mineral separates from previously characterised samples of the Heise rhyolites (e.g. Bindeman *et al.*, 2007) to test our correlations (see below) and determined the oxygen isotope compositions of the drillcore rhyolites via analyses of sanidine, quartz, and clinopyroxene (Fig. 9). The re-analysed samples from the surficial stratigraphy show excellent agreement with published values for these units. The previously unanalysed Winnetou Tuff sample returned the lowest $\delta^{18}\text{O}$ of all samples analysed in this study, with sanidine values of 1.41‰ and 1.35‰ and clinopyroxene of 0.37‰, in mutual high-temperature equilibrium. The $\delta^{18}\text{O}$ value for

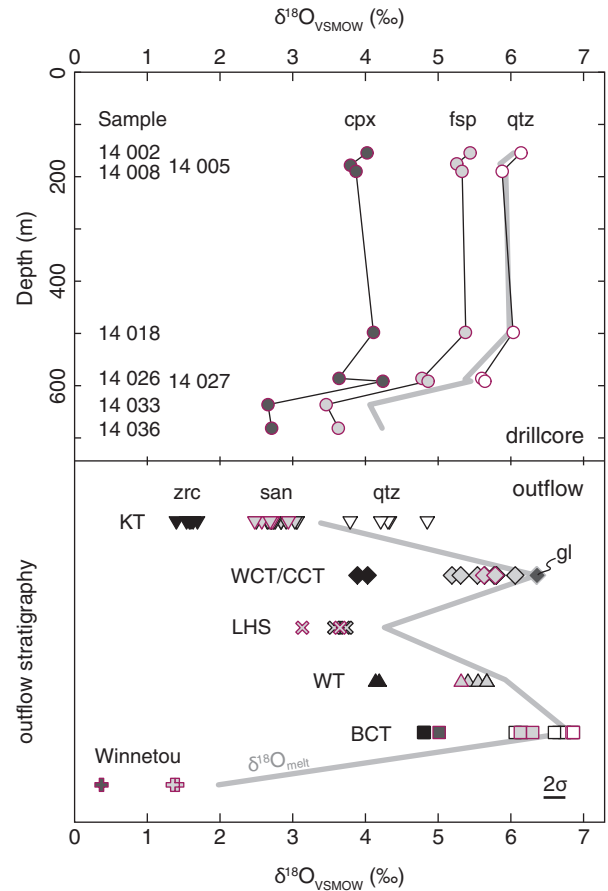


Fig. 9. Oxygen isotopic compositions of minerals from the Heise rhyolites, including new results (purple rims) and data from Watts *et al.* (2011) (black rims). Fill colours denote the phase analysed: white, quartz; light grey, sanidine; dark grey, clinopyroxene; black, zircon; dark grey with bright rim, glass. The thick grey line is an approximate $\delta^{18}\text{O}_{\text{melt}}$ based on $\Delta^{18}\text{O}_{\text{melt-sanidine}} = 0.6\%$ (Bindeman *et al.*, 2001).

this unit indicates that it is not equivalent to the normal- $\delta^{18}\text{O}$ tuff of Lost River Sinks that Drew *et al.* (2013) reported underlying the tuff of Blacktail Creek, but rather represents a separate deposit defined here on the basis of $\delta^{18}\text{O}$ and mineralogy. In the drillcore rhyolites, the quartz–sanidine–pyroxene O isotopic compositions are consistent with high-temperature fractionation, indicating that these minerals have not been modified by post-eruptive alteration processes and crystallised from low- $\delta^{18}\text{O}$ magmas. Throughout the drillcore quartz varies from 5.60 to 6.14‰, sanidine from 3.46 to 5.44‰, and pyroxene from 2.66 to 4.24‰ (Fig. 9). The uppermost samples from the drillcore, ranging from ~ 150 to ~ 500 m in depth, have similar $\delta^{18}\text{O}$ values (quartz, sanidine and pyroxene). Samples 14 026 and 027 have $\delta^{18}\text{O}$ values about 0.5‰ lower than those for the stratigraphically higher rhyolites, and the basal rhyolites 14 033 and 14 036 have values a further $\sim 1\%$ lower. Notably, none of the post-Kilgore Tuff rhyolites within the drillcore have sanidine compositions comparable with those we determined for the Kilgore Tuff ($\delta^{18}\text{O}$ 2.48–2.94‰, $n=5$).

Overall, quartz, sanidine and pyroxene in the rhyolites from the drillcore show a subtle increase in $\delta^{18}\text{O}$ values with decreasing depth and start with values higher than those for the Kilgore Tuff (Fig. 9).

Bulk samples

Whole-rock powders from the visibly altered portion of the drillcore (14 029, 030, 031) yield a wide range of $\delta^{18}\text{O}$ between -3.5‰ and 1.0‰ and two unaltered samples (14 002 and 018) return values of 5.9‰ and 6.5‰ respectively. The bulk values closely approximate the predicted magma values based on the laser fluorination data and using $\Delta^{18}\text{O}_{\text{melt-sanidine}}$ of 0.6‰ (Bindeman *et al.*, 2001), emphasising the fresh nature of samples 14 002 and 018.

Pb isotopes

$^{208}\text{Pb}/^{206}\text{Pb}$ and $^{207}\text{Pb}/^{206}\text{Pb}$ ratios in sanidine and glass reveal substantial isotopic variability between the Heise magmas, with a range spanning $\sim 2.10\text{--}2.26$ in $^{208}\text{Pb}/^{206}\text{Pb}$ and $\sim 0.85\text{--}0.91$ in $^{207}\text{Pb}/^{206}\text{Pb}$ (Fig. 10). Within the relatively poor precision of the measurement by LA-ICP-MS, sanidine compositions show unimodal distributions characteristic for each unit across all sampling localities, with samples clustering into distinct fields for particular units. In each case, there is no distinguishable isotopic difference between sanidine occurring as single homogeneous crystals and that which is found surrounding cores of plagioclase (Fig. 4). Interestingly, the rhyolites from the drillcore are compositionally distinct from the outflow Heise rhyolites, with compositions higher in both $^{208}\text{Pb}/^{206}\text{Pb}$ and $^{207}\text{Pb}/^{206}\text{Pb}$ suggesting a lower influence of crustal materials in their genesis. As with previous data (e.g. plagioclase trace elements, pyroxene compositions, oxygen isotopes), the Winnetou ignimbrite is somewhat distinct in its Pb isotope composition, plotting off the trend described by the Heise magmas.

Geochronology

Zircons separated from rhyolite from three levels in the drillcore (samples 14 002, 018 and 036) were dated by SIMS and the basal unit 14 036 was additionally dated by ID-TIMS to refine the temporal relationship between the interval retrieved from the drillcore and outcropping units (Fig. 11). SIMS U–Pb dates for the three samples indicate an affinity with the Heise centre, with weighted mean $^{206}\text{Pb}/^{238}\text{U}$ dates of 3.86 ± 0.19 Ma for sample 14 002 (MSWD = 0.95, $n = 8/10$) and 3.74 ± 0.15 Ma for sample 14 018 (MSWD = 0.99, $n = 10/10$). Zircon crystals from lowest sample 14 036 returned a SIMS U–Pb date of 4.44 ± 0.19 Ma (MSWD = 3.79, $n = 9/10$, omitting one crystal with a date of 6.48 Ma) and an ID-TIMS U–Pb date of 4.0248 ± 0.0011 Ma (MSWD = 0.68, $n = 8/10$). The weighted average of the SIMS dates for sample 14 036 is strongly biased by two high-U spots (>10000 ppm U); omitting these spots yields a weighted average U–Pb date of 4.10 ± 0.25 Ma, which is in agreement with the

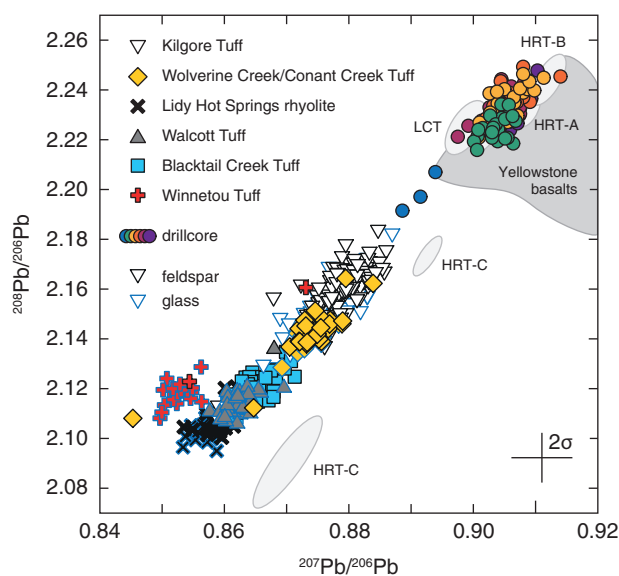


Fig. 10. Lead isotopic compositions of sanidine and glass from the Heise rhyolites illustrating the differences between major ignimbrites and the drillcore units. For comparison, fields of Yellowstone basalts, Huckleberry Ridge Tuff (HRT; members A, B, and C) and Lava Creek Tuff (LCT) are reproduced from Watts *et al.* (2012).

ID-TIMS date. Collectively, the SIMS and ID-TIMS U–Pb dates constrain the age of the base of the drillcore and characterise the studied core interval as a post-Kilgore Tuff sequence (4.4876 ± 0.0023 Ma; Wotzlaw *et al.*, 2014; Fig. 11).

Both the SIMS and ID-TIMS datasets contain rare analyses with $^{206}\text{Pb}/^{238}\text{U}$ dates significantly older than the main population that were excluded from the weighted mean calculation. These zircon dates are interpreted to be related to recycled antecrystic or xenocrystic zircons, with one of the zircons in sample 14 036 (6.48 ± 0.51 Ma) probably from the oldest regional Heise ignimbrite, the 6.62 Ma Blacktail Creek Tuff (Morgan & McIntosh, 2005).

Geothermometry

Zircon saturation thermometry [via Watson & Harrison (1983), used for direct comparison with Watts *et al.* (2011)] returned temperatures between 797 and 895°C, showing excellent agreement with previous studies. Notably, the highest temperature returned is from the Winnetou ignimbrite, further suggesting that this unit may belong to the typically hotter rhyolites of the central Snake River Plain (Honjo *et al.*, 1992; Cathey & Nash, 2004). Overall, two-pyroxene thermometry (Andersen *et al.*, 1993) returned temperatures (848–902°C) higher than the zircon-saturation thermometry in all cases. Fe–Ti oxide temperatures (Henshaw, 2002) either overlap with two-pyroxene temperatures or are somewhat cooler, as previously demonstrated by Honjo *et al.* (1992) for the rhyolites of the CSRP. Temperatures for the drillcore samples show no significant distinction from those for the outflow stratigraphy,

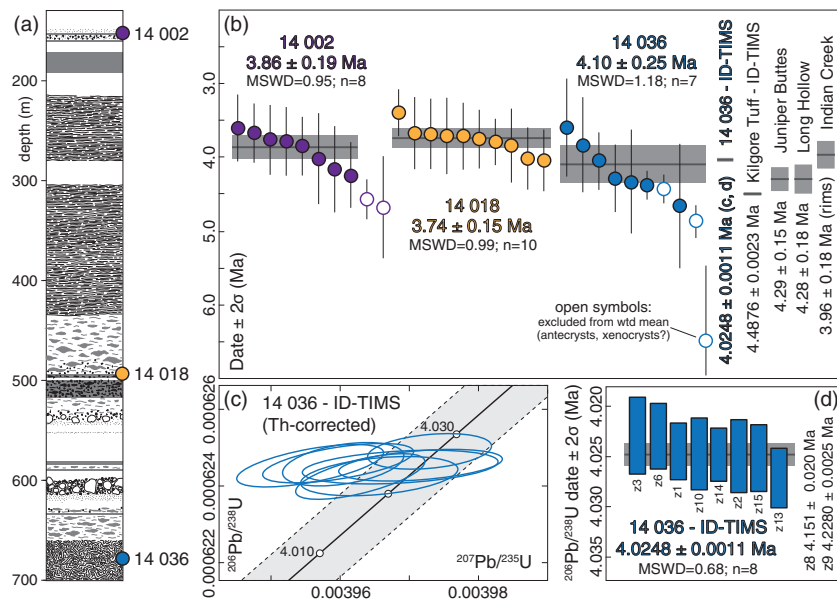


Fig. 11. U-Pb geochronology of zircons from the Sugar City drillcore: (a) stratigraphic positions of dated samples. (b) SIMS U-Pb zircon ages compared with previously published ages of post-Kilgore Tuff rhyolites (Bindeman *et al.*, 2007). (c) ID-TIMS concordia diagram and (d) age-ranked ID-TIMS $^{206}\text{Pb}/^{238}\text{U}$ zircon ages of the lowest sample found in the core (14 036) with single zircons referred to as z1, etc. The entire succession of rhyolites exposed in the core ranges in age between 4.02 and 3.86 Ma and is younger than the youngest regional ignimbrite, the Kilgore Tuff. The stratigraphically lowest rhyolite, although overlapping within uncertainty with the Kilgore Tuff for the SIMS measurements, returns a precise TIMS age of 4.0248 ± 0.0011 Ma, which is significantly younger than the Kilgore Tuff at 4.4876 ± 0.0023 Ma (Wotzlaw *et al.*, 2014). Also shown for comparison in (b) are the ages of the post-Kilgore rhyolitic lavas, Juniper Buttes, Long Hollow and Indian Creek (Watts *et al.*, 2011), that are exposed on the surface.

indicating the persistence of high-temperature volcanism throughout the 3 Myr history of the Heise volcanic field. Temperatures determined via quartz-clinopyroxene O isotope thermometry for the drillcore rhyolites range between 861 and 925°C, similar to temperatures calculated for the Kilgore Tuff (917°C) and the Blacktail Creek Tuff (880°C) using the same method (Loewen & Bindeman, 2016).

DISCUSSION

Rhyolite stratigraphy at Heise

Based on the compositional and geochronological information described above, we are able to split the rhyolite from the drillcore into compositionally distinct units. In the upper part of the drillcore, the complete overlap in trace elements in glasses and major elements in pyroxenes makes a strong case that samples 14 002 to 14 021 represent a single magma batch. This is supported by the identical U–Pb SIMS dates for zircons from samples 14 002 and 14 018. A second magma batch is defined by samples 14 026 and 14 027, which show distinctly different pyroxene and glass compositions (Figs 3 and 8) and a coherent change in the $\delta^{18}\text{O}$ of all phases measured (Fig. 9). Texturally, these samples are distinct from the overlying rhyolite as they contain ~14% crystals rather than 5–8% in the 14 002 to 14 021 unit (point counting data and images of thin sections are given in the Supplementary Data). Beneath this, it is clear that sample 14 033 is distinct

from 14 026 and 14 027 (in terms of pyroxene compositions, glass compositions, and crystallinity), whereas the relationship between 14 033 and 14 036 is less certain: they have similar crystallinities and pyroxene compositions (at least in terms of augite) but the limited Pb isotope data for 14 036 suggest that it may be different. Despite this, and for the sake of simplicity, we prefer to group 14 033 and 14 036 as representing the same magma batch with the acknowledgement that with further work they may turn out to differ. Overall, we split the drillcore into the Upper Rhyolite (samples 14 002 to 14 021), the Middle Rhyolite (samples 14 026 to 14 027), and the Lower Rhyolite (samples 14 033 to 14 036).

With the wealth of new compositional and chronological information presented above, new insights are gained into the Heise volcanic field. A first-order observation is that the rhyolites in the Sugar City drillcore do not yet have a known surficial expression around the Heise volcanic field and, conversely, none of the rhyolites that have been characterised on the surface appear in the drillcore. The ability to confidently correlate magma batches via geochemical and petrological means requires that the magma batches themselves are not compositionally zoned. Whereas zonation is a relatively common occurrence in rhyolites from subduction zones (e.g. Hildreth, 1981; Bacon & Druitt, 1988; Hildreth & Wilson, 2007), it is very limited in the hot, dry rhyolites of the Snake River Plain [see Wolff *et al.* (2015) for a thorough treatment of this issue]. To illustrate the reliability of geochemical correlation, we use our new

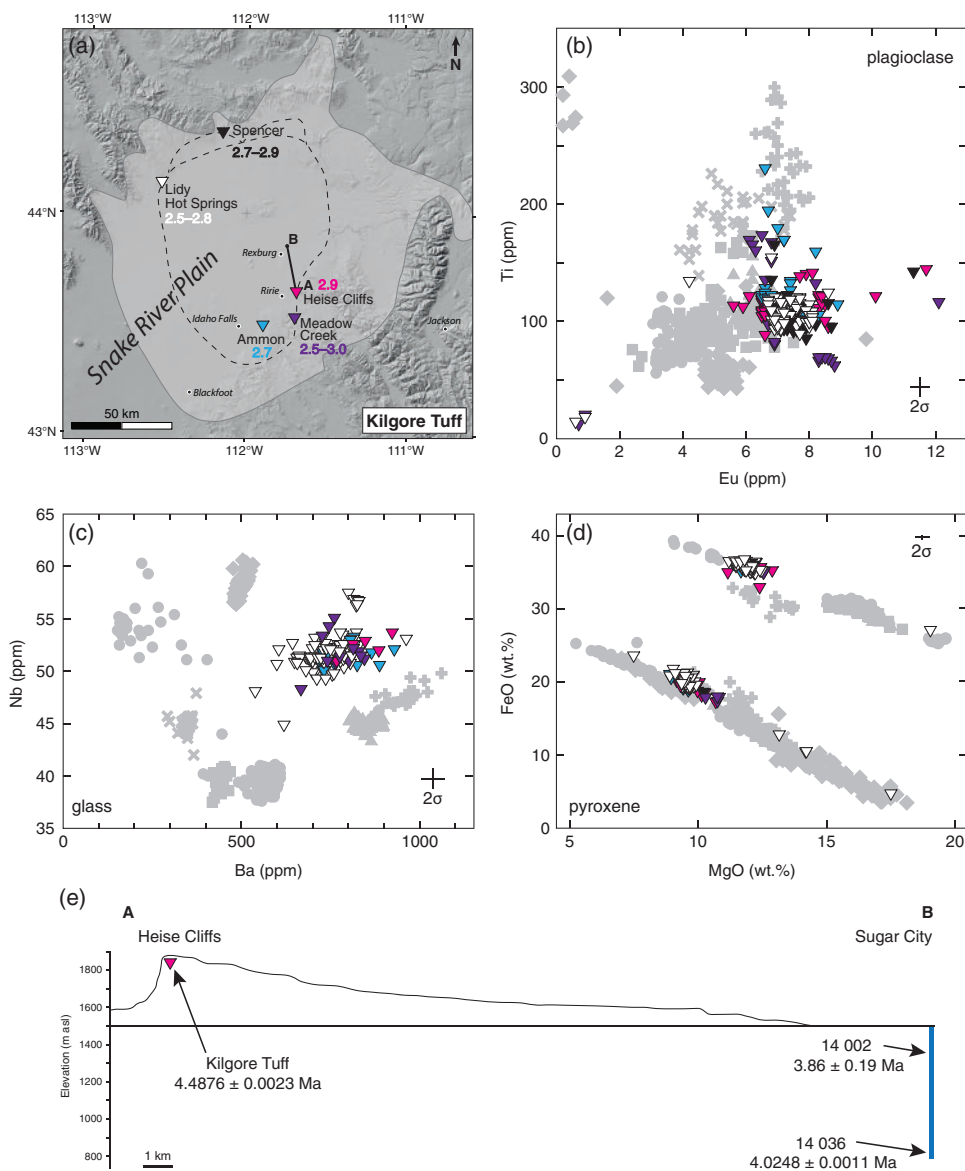


Fig. 12. Chemical signatures of minerals and glass from five samples of Kilgore Tuff collected on both margins of the Snake River Plain. (a) Sample localities with sanidine $\delta^{18}\text{O}$ ranges from this study and [Watts *et al.* \(2011\)](#). (b) Plagioclase trace elements, (c) glass trace elements, (d) pyroxene major elements compared with all other samples from this study coloured grey. (e) Simplified cross-section from the Heise Cliffs outcrop to Sugar City illustrating the requirement of a significant drop of the intracaldera block to explain the offset in stratigraphy. Zircon U–Pb ages are from this study and [Wotzlaw *et al.* \(2014\)](#).

data for the most widely dispersed Heise ignimbrite, the Kilgore Tuff ([Fig. 12](#)). Figures in the Results section that display Kilgore Tuff data (e.g. [Figs 3, 4, 6 and 8](#)) are based on the combination of five samples taken from widely separated locations. When Kilgore Tuff samples are plotted by sample location, they overlap completely in glass, feldspar and pyroxene compositions ([Fig. 12](#)) and, importantly, these parameters distinguish the Kilgore Tuff from other Heise ignimbrites. Further, the O isotopic compositions of these samples overlap within a narrow range and are in good agreement with previous work ([Bindeman *et al.*, 2007](#); [Watts *et al.* 2011](#)). Finally, independent studies have found identical compositional and chronological records in zircon from

across the Kilgore Tuff ([Wotzlaw *et al.*, 2014](#)). Our findings suggest that major elements in pyroxene and trace elements in glasses and plagioclase are most distinctive of a magma batch in the Snake River Plain (cf. [Anders *et al.*, 2014](#)).

An intracaldera record

Throughout the central Snake River Plain, the sources of the voluminous ignimbrites are poorly known and the calderas are commonly assumed to be buried by younger basalts ([Bonnichsen *et al.*, 2008](#); [Branney *et al.*, 2008](#)). In contrast, the relative youth of the currently active Yellowstone volcanic field allows intracaldera

processes, including abundant hydrothermal activity and the eruption of numerous rhyolitic lavas and rare pyroclastic deposits (Vazquez *et al.*, 2009; Stelten *et al.*, 2013), to be observed as a potential analogue to the Heise volcanic field and the Sugar City drillcore.

Given the location of the Sugar City drillcore within the Snake River Plain and within the Kilgore Tuff caldera margins, as suggested by Morgan & McIntosh (2005), the absence of the Kilgore Tuff within the core requires explanation. The Kilgore Tuff tops the succession at the Heise Cliffs location (Phillips *et al.*, 2016; Fig. 12), 25 km to the south of Sugar City, and yet the bottom of the drillcore does not reach the Kilgore Tuff. If the distribution of the Kilgore Tuff is as previously suggested (e.g. Morgan & McIntosh, 2005; Watts *et al.*, 2011; and supported by our correlations above), this would require a drop in elevation of ≥ 1 km passing north. An offset of this magnitude is not unusual for caldera faults and has been widely documented; many examples in the western USA have between 1 and 3 km of offset (e.g. Lipman, 1984; Spray, 1997). We note here that the path between the Heise Cliffs location and the Sugar City drillcore (illustrated in Fig. 12) does not cross any of the broadly north–south-trending Basin and Range faults. Further, in many cases, particularly those to the north of the plain, the Miocene volcanic rocks onlap topography created by Basin and Range faulting rather than being disrupted by it. In light of this, we propose that the down-dropping observed may be produced by crossing a caldera fault (or faults) within the plain.

Ponding of drillcore ignimbrites

Commonly (although this remains dependent upon the timing of caldera collapse in the specific case), calderas are filled by thick ignimbrites produced during the same event, with extracaldera deposits usually significantly thinner (e.g. Lipman, 1997). Within the drillcore succession, the Upper Rhyolite is at least 300 m thick, and unlike some portions of the core, it is unequivocally pyroclastic in origin as illustrated by the abundant fiamme and lithic clasts in the basal third of this unit. Yet our extensive characterisation of the outflow succession associated with the Heise volcanic centre reveals that the Upper Rhyolite is not found on the margins of the plain. Given that unconfined pyroclastic density currents tend to produce ignimbrites with gently sloping upper surfaces (e.g. Branney & Kokelaar, 2002) that feather out laterally or onlap pre-existing topography, the absence of the Upper Rhyolite would suggest that it was constrained by topography as would be expected within a caldera setting (e.g. Kokelaar *et al.*, 2007). Indeed, the Upper Rhyolite is considerably thicker than outflow ignimbrite sheets from either Heise or the central Snake River Plain, which are ≤ 150 m thick and mostly < 100 m thick. By way of comparison, the thickness of the Upper Rhyolite within the drillcore is similar to the intracaldera thicknesses of the Yellowstone ignimbrites (Huckleberry Ridge Tuff A—

200 m, B—150 m, and C—350 m; Lava Creek Tuff A—400 m and B—300 m; Mesa Falls Tuff—150 m) as estimated by Christiansen (2001). We note, however, that in many cases the bases of these intracaldera successions at Yellowstone are not exposed, allowing for these deposits to be significantly thicker, more similar to those interpreted as intracaldera from elsewhere in the province (e.g. McCurry & Rodgers, 2009). Regardless of this, the Upper Rhyolite remains significantly thicker than any extracaldera ignimbrite known in the YSRP.

Hydrothermal alteration

The occurrence of hydrothermally altered portions of rhyolite (see below) within the drillcore (samples 14 029, 030, 031) further suggests that the Sugar City core is penetrating an intracaldera succession. Hydrothermal alteration is a common feature within calderas globally, with the hydrothermal system at Yellowstone being one of the best studied, particularly in the shallowest portions (e.g. Lowenstern *et al.*, 2006, and references therein). Notably, the vast majority of outflow rhyolites from the Snake River Plain and Yellowstone are entirely hydrothermally unaltered (Bonnichsen *et al.*, 2008). Hydrothermally altered intracaldera rocks are well documented from Yellowstone (e.g. Bargar & Beeson, 1985) with bulk $\delta^{18}\text{O}$ values reaching as low as -4.3% similar to the -3.5% of sample 14 031 (Hildreth *et al.*, 1984; Sturchio *et al.*, 1986). A variety of minerals (quartz, chalcedony, cristobalite, and calcite) from hydrothermal veins have $\delta^{18}\text{O}$ values reaching as low as -8.7% (Hildreth *et al.*, 1984; Sturchio *et al.*, 1990). The similarity in terms of bulk $\delta^{18}\text{O}$ of the altered samples from Yellowstone and Heise suggests that Yellowstone represents a reasonable potential analogue for the Heise eruptive centre.

Cannibalisation and rhyolite generation at Heise

The petrogenesis of the rhyolites of the Heise centre and surroundings has been much discussed, with the majority of attention focused on the low- $\delta^{18}\text{O}$ values of the youngest rhyolitic magmas (Bindeman *et al.*, 2007; Watts *et al.*, 2011; Boroughs *et al.*, 2012; Wotzlaw *et al.*, 2014) and temporal variations in $\delta^{18}\text{O}$. Briefly, the model of cannibalisation proposed for Heise involves the intracaldera portions of older (yet still Miocene) rhyolites undergoing high-temperature hydrothermal alteration before being down-dropped and buried by a series of at least 2–3 subsequent caldera-forming events. Eventually, these hydrothermally altered rhyolites arrive at sufficient depths to undergo partial melting and generate low- $\delta^{18}\text{O}$ silicic magmas with heterogeneous zircon cargoes (e.g. Bindeman & Simakin, 2014; Wotzlaw *et al.* 2014). Eventually this source material is exhausted and the magmas recover to normal $\delta^{18}\text{O}$ values. This model explains well the generation of low- $\delta^{18}\text{O}$ magmas relatively late in the development of the Heise (and Yellowstone) volcanic fields, and the increase in magma $\delta^{18}\text{O}$ value on

passing upward through the core is also consistent with a post-Kilgore recovery stage (e.g. Bindeman *et al.*, 2007; Fig. 9). The Upper Rhyolite in the drillcore is younger than, or overlaps in age with, the other post-Kilgore effusive volcanism (the Long Hollow, Indian Creek and Juniper Buttes rhyolites), which all have lower $\delta^{18}\text{O}$ (3.44–3.86‰, Watts *et al.*, 2011) than observed in samples from the drillcore (Upper Rhyolite 5.25–5.44‰ and Middle Rhyolite 4.77–4.85‰; all values are from sanidine for comparison). The patterns of $\delta^{18}\text{O}$ and the discovery of buried hydrothermally altered material in the drillcore together provide strong support for the cannibalisation model at Heise.

Altered samples 14 029, 030, and 031 display XRD spectra that are much more complex than those for either the unaltered rhyolites that surround them in the drillcore or the microcrystalline interiors of rhyolites observed on the surface (Fig. 13). The XRD spectra for these visibly altered rocks support the presence of chlorite and epidote, which are not found in the fresh rhyolites. Quartz–epidote–chlorite alteration facies constrain temperatures to be $>150\text{--}300^\circ\text{C}$ (Browne, 1978) and at such high temperatures mineral–water isotope fractionations are low; thus the rock moves towards the low $\delta^{18}\text{O}$ values of isotopically unshifted meteoric water. These samples have bulk $\delta^{18}\text{O}$ values of 1.0‰, 0.1‰, and -3.5% , lower than the pristine rhyolites, which have bulk $\delta^{18}\text{O}$ of 5.9–6.7‰ (Figs 9 and 13). Importantly for the cannibalisation model, these altered samples are demonstrably related to the Heise volcanic field, being constrained by U–Pb ages older than 14 018

(3.74 ± 0.15 Ma, via SIMS) and younger than 14 036 (4.0248 ± 0.0011 Ma, via ID-TIMS).

To test whether such hydrothermally altered rocks are geochemically suitable source materials for low- $\delta^{18}\text{O}$ rhyolites at Heise, major and trace elements from the altered samples were compared with their unaltered equivalents. Although generally similar to the fresh Heise volcanic rocks, the altered samples do show some differences in major elements (e.g. lower Na_2O throughout, elevated SiO_2 in 14 030, and elevated CaO in 14 031). In terms of trace elements, the altered samples also show considerable overlap with unaltered samples both for potentially fluid-mobile elements (e.g. Rb, Ba; Fig. 14) and for relatively immobile elements such as the REE (Fig. 14). Broadening the comparison to include the hydrothermally altered samples from Yellowstone drillcores (Beeson & Bargar, 1984; Sturchio *et al.*, 1986), some differences are observed. In general, the samples from Yellowstone drillcores extend to lower Rb and Ba contents than the altered Heise samples (Fig. 14). This difference could be a function of a somewhat larger sample set for Yellowstone, where the drilling focused on hydrothermally altered areas, or may be the result of a slightly different alteration regime in Yellowstone. Regardless, it is noteworthy that the degree of depletion in $\delta^{18}\text{O}$ is unrelated to trace element variations. Overall, the absence of a stark compositional change associated with the hydrothermal alteration of the Heise samples indicates that they may prove suitable source materials for the low- $\delta^{18}\text{O}$ rhyolites. The

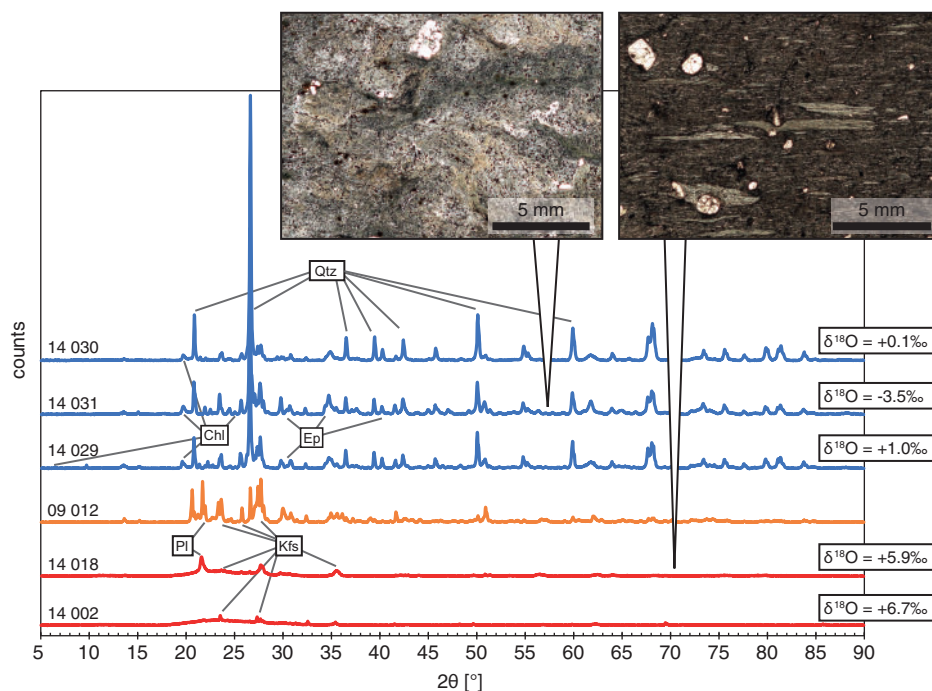


Fig. 13. X-ray diffraction spectra and bulk $\delta^{18}\text{O}$ values of hydrothermally altered Sugar City drillcore rhyolites (blue) compared with unaltered glassy (red, drillcore samples) and devitrified rhyolites (yellow, Tuff of Knob from the central Snake River Plain; Rowe *et al.*, 2012). XRD peak positions are marked with characteristic minerals; for example, chlorite (Chl) and epidote (Ep) representing the alteration assemblage. Inset photographs show the appearance of fresh and hydrothermally altered rhyolitic ignimbrites in thin section.

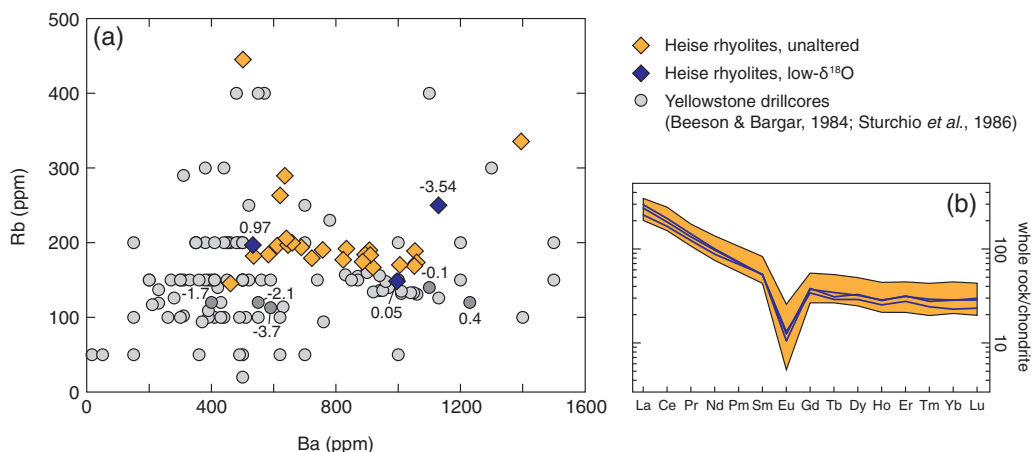


Fig. 14. Geochemical comparison of hydrothermally altered samples from Yellowstone and Heise and the unaltered rhyolites. (a) Relatively fluid-mobile elements illustrating overlap between unaltered and altered samples from Heise. Also shown are altered samples from Yellowstone, which extend to lower Ba and Rb contents. Numbers associated with darker symbols are either bulk or groundmass $\delta^{18}\text{O}$ values (in ‰) showing no relationship between trace element abundance and $\delta^{18}\text{O}$. (b) REE patterns illustrating similarity between altered and unaltered samples at Heise.

following section explores this suggestion in more detail via numerical modelling.

Rhyolite-MELTS constraints on petrogenesis

To investigate the petrogenesis of the low- $\delta^{18}\text{O}$ rhyolites and their pre-eruptive storage conditions we performed simulations using rhyolite-MELTS (Gualda *et al.*, 2012), with the results evaluated in the light of experimental studies and thermobarometric data. Here we focus on the generation of the Kilgore Tuff, as the most voluminous low- $\delta^{18}\text{O}$ rhyolite of the Heise volcanic field (Bindeman *et al.*, 2007).

In Heise, the early stages of rhyolite petrogenesis are recorded in the form of intermediate melt inclusions hosted in augite crystals that have higher Mg# (~60–90) and lower REE contents with a prominent lack of Eu anomalies compared with typical pyroxenes from Heise rhyolites (Szymanowski *et al.*, 2015). These melt inclusions have been interpreted as representing the intermediate differentiation product between the basalt and rhyolite end-members and thus provide important constraints on the magmas feeding the parental reservoir to the widely erupted rhyolite magmas in Heise.

Equilibrium testing between these melt inclusions and their host augites (Putirka, 2008) reveals disequilibrium either in the $K_D(\text{Fe-Mg})$ or the normative pyroxene components and we find that rhyolite-MELTS will not stabilise augite for most of the melt inclusion compositions, even when a wide range of possible P – T – H_2O – $f\text{O}_2$ conditions is explored. Szymanowski *et al.* (2015) described the potential for post-entrapment crystallisation that will shift glass compositions away from the normative augite composition and thus reduce their capacity to saturate augite. By back-adding up to 5% host augite composition to the composition of the melt inclusion, the melt composition prior to post-entrapment crystallisation can be approximated. The recalculated

augite–melt pairs now fulfil at least one of the equilibrium tests that are used in cpx–liquid thermometry [Putirka, 2008; $K_D(\text{Fe-Mg}) = 0.28 \pm 0.08$, $\Delta\text{DiHd}_{\text{observed-predicted}} < 0.2$], with four pairs fulfilling both requirements returning $1017 \pm 19^\circ\text{C}$ [equation (33) of Putirka (2008)] at 4.5 ± 0.7 kbar [equation (32c) of Putirka (2008), independent of the initial H_2O content of the melt]. These conditions are in agreement with calculations in rhyolite-MELTS, where at pressures of 4.0–4.5 kbar an average melt inclusion corrected for 5% of post-entrapment crystallisation will stabilise augite at 1020–1030°C for water contents of 0.4–0.6 wt %. The pressure estimates are consistent both with the base of the current rhyolite magma reservoir in Yellowstone as geophysically imaged (8–18 km; Husen *et al.*, 2004) and with the mid-crustal sill imaged in the eastern Snake River Plain (Peng & Humphreys, 1998), which has been interpreted as a mafic cumulate by Shervais *et al.* (2006).

The O isotopic composition of the Kilgore Tuff magma is 3.3–3.6‰ (relative to VSMOW), significantly lower than the value of $+6.3 \pm 0.3\text{‰}$ that would be expected from closed-system fractionation of a basalt (Bindeman, 2008). If we assume that the hydrothermally altered rhyolite in the drillcore is equivalent to the material that was assimilated during the petrogenesis of the Kilgore Tuff, we can use O isotopes to bracket the degree of assimilation required to between 26 and 54% (taking $\delta^{18}\text{O} = 6.0\text{‰}$ as the starting composition and using the end-member drillcore compositions of $\delta^{18}\text{O} = 1.0\text{‰}$ and -3.5‰). Evolutionary paths involving assimilation and concurrent fractional crystallisation can be modelled via rhyolite-MELTS by using the back-calculated average composition of the melt inclusions described above as the starting composition and the average composition of hydrothermally altered rhyolite found in the drillcore as assimilants (Fig. 15). Assimilation is probably confined to shallow depths where buried hydrothermally altered material is abundant, therefore we take the magmatic

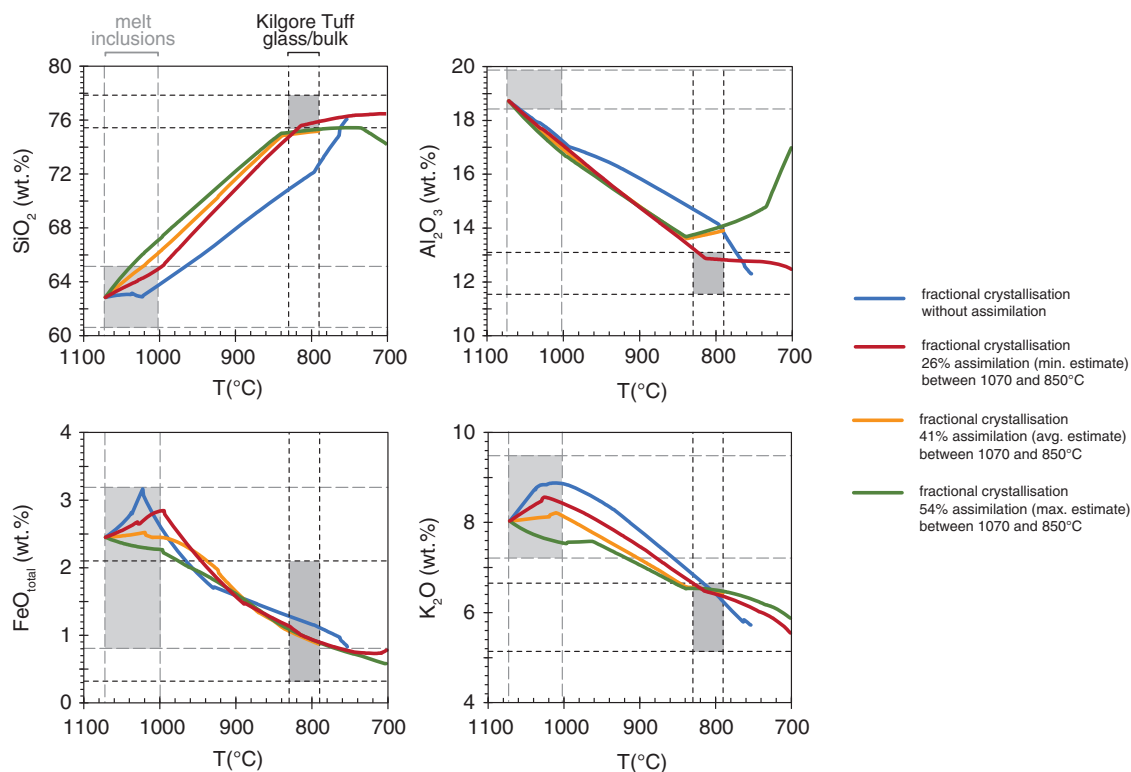


Fig. 15. Results of rhyolite-MELTS simulations. Grey boxes represent the compositions of the intermediate melt inclusions as the starting point and the Kilgore Tuff as the end product. The simulations shown (see Supplementary Data) well approximate the Kilgore Tuff compositions with the range of assimilant constrained from the bulk and O isotopic compositions of drillcore samples 14 029 to 14 031.

storage conditions likely for the Kilgore Tuff [1.5 kbar; quartz–fayalite–magnetite (QFM)] as parameters during assimilation. This choice of pressure is based upon experimental work on Heise rhyolites by Bolte *et al.* (2015), who identified storage conditions of the Blacktail Creek Tuff as 845–875°C, 1.3–2.5 kbar, and 1.5–2.5 wt % H₂O close to the QFM buffer. When assimilating 40–50% of low- $\delta^{18}\text{O}$ rhyolite melt over a temperature range of 220°C starting with the liquidus of the melt inclusion composition ($\sim 1070^\circ\text{C}$), we can adequately reproduce Kilgore-type melt compositions at the temperatures indicated via geothermometry ($\sim 800\text{--}900^\circ\text{C}$; see ‘Geothermometry’ and Supplementary Data). We note that the 830°C Fe–Ti oxide temperature (Henshaw, 2002), commonly inferred to represent the most accurate eruptive temperature, lies towards the lower end of this range. Temperature and water content estimates are consistent with results from plagioclase–melt hygrometry (Waters & Lange, 2015) of 3.1 ± 0.35 wt % H₂O (uncertainty using standard error of estimate on regression) at 1.5 kbar and 820°C. Phases crystallising in the rhyolite-MELTS simulations include the typical Heise mineral assemblage of sanidine + plagioclase + quartz + Fe–Ti oxides + Opx \pm Cpx. The results can be equally reproduced in isenthalpic mode where temperature is controlled by the rate of assimilation, the temperature of the assimilant and the latent heat released by crystallisation,

although unrealistically high assimilant temperatures of $>700^\circ\text{C}$ would be required to assimilate $>40\%$ material.

CONCLUSIONS

The main conclusions of our study are as follows.

1. By combining multiple geochemical and isotopic characteristics, we can confidently distinguish magma batches in the YSRP system. Based on our geochemical library of thousands of new analyses, we prefer the use of major elements in pyroxenes, trace elements in glasses and trace elements in plagioclase to distinguish magma batches. Pb isotopes and O isotopes within a magma batch may be helpful, but are better considered circumstantial evidence. Given the large overlap in compositions between the units illustrated here, we do not recommend attempting to use major elements in feldspars for magma discrimination in the Snake River Plain (see Anders *et al.*, 2014).
2. The oldest outflow ignimbrite we sampled, the informally named Winnetou Tuff, is not typical of the other rhyolites in this study. The Winnetou unit contains pigeonite together with orthopyroxene, and returns a high magmatic temperature. Additionally, this unit has extremely low $\delta^{18}\text{O}$ of 1.4‰ in sanidine

and plots in a subtly different space in terms of Pb isotopes. Taken together, these differences suggest that the Winnetou Tuff has an affinity with the rhyolites of the central Snake River Plain and so may be used to define the start of 'Heise volcanism'.

3. The combination of mineral and glass geochemistry and U-Pb SIMS and ID-TIMS geochronology reveals that the outflow succession from the Heise eruptive centre is not preserved within the drillcore, nor have any of the drillcore rhyolites yet been found at the surface. The absence of the Kilgore Tuff in the drillcore succession requires it be down-dropped at least 1 km from where it is exposed on the Heise Cliffs (Fig. 12). The absence of the thick Upper Rhyolite ignimbrite within the surficial stratigraphy suggests that the drillcore penetrates an intra-caldera succession. This interpretation is strengthened by the occurrence of hydrothermally altered lithologies within the drillcore.
4. Synoptically, the data from the drillcore provide strong support for the 'cannibalisation' model of petrogenesis that has been proposed for the Heise volcanic centre. First, the pyroxene–sanidine–quartz $\delta^{18}\text{O}$ compositions of the rhyolites in the drillcore, although low, are higher than in the preceding Kilgore Tuff. This increase in $\delta^{18}\text{O}$ would be consistent with a recovery stage (as inferred for Yellowstone) as the hydrothermally altered source material is progressively exhausted. Second, the presence of 'Heise-aged' hydrothermally altered rhyolite in the drillcore (as defined by U-Pb geochronology) illustrates the potential for suitably altered source materials to be buried by subsequent volcanism as predicted by the cannibalisation model.
5. Kilgore Tuff compositions can be reproduced via rhyolite-MELTS models using an intermediate melt as a starting material with subsequent fractionation and assimilation of the hydrothermally altered materials described in this study. These models, with degrees of assimilation constrained by the O isotopic compositions of assimilants, show best matches with 40–50% assimilation.

SUPPLEMENTARY DATA

Supplementary data for this paper are available at *Journal of Petrology* online.

ACKNOWLEDGEMENTS

This work, particularly the sampling of the drillcore, would not have been possible without the kind assistance from Linda Davis (US Geological Survey) and Mary Hodges (Idaho National Laboratory). Bill Phillips (Idaho Geological Survey) helped with sampling and provided valuable insights into Heise volcanism and Idaho geology in general. Marlon Jean provided useful input to an early draft of this paper. Constructive and thoughtful journal reviews from George Cooper and

Calvin Miller are gratefully acknowledged in improving this work. Editor Wendy Bohrsen provided valuable comments, a critical eye, and suggestions for models. Sherissa Roopnarain assisted with the whole-rock O-isotope analyses.

FUNDING

J.F.W. acknowledges funding through the ETH Zurich postdoctoral fellowship program. I.N.B. acknowledges support from NSF grant EAR-1447337. Funding for the ETH group is from SNF grants SNSF 200021_146268 and SNSF 200021_155923. The ion microprobe facility at UCLA is partly supported by a grant from the Instrumentation and Facilities Program, Division of Earth Sciences, National Science Foundation. Whole-rock O-isotope analyses were funded by NRF incentive grants to C.H.

REFERENCES

- Anders, M. H., Rodgers, D. W., Hemming, S. R., Saltzman, J., DiVenere, V. J., Hagstrum, J. T., Embree, G. F. & Walter, R. C. (2014). A fixed sublithospheric source for the late Neogene track of the Yellowstone hotspot: Implications of the Heise and Picabo volcanic fields. *Journal of Geophysical Research: Solid Earth* **119**, 2871–2906.
- Andersen, D. J., Lindsley, D. H. & Davidson, P. M. (1993). QUILF: a Pascal program to assess equilibria among Fe–Mg–Mn–Ti oxides, pyroxenes, olivine, and quartz. *Computers and Geosciences* **19**, 1333–1350.
- Annen, C. & Sparks, R. S. J. (2002). Effects of repetitive emplacement of basaltic intrusions on thermal evolution and melt generation in the crust. *Earth and Planetary Science Letters* **203**, 937–955.
- Bachmann, O. & Bergantz, G. W. (2003). Rejuvenation of the Fish Canyon magma body: A window into the evolution of large-volume silicic magma systems. *Geology* **31**, 789–792.
- Bachmann, O. & Bergantz, G. (2004). On the origin of crystal-poor rhyolites: extracted from batholithic crystal mushes. *Journal of Petrology* **45**, 1565–1582.
- Bachmann, O. & Bergantz, G. (2008). Rhyolites and their source mushes across tectonic settings. *Journal of Petrology* **49**, 2277–2285.
- Bacon, C. R. & Druitt, T. H. (1988). Compositional evolution of the zoned calcalkaline magma chamber of Mount Mazama, Crater Lake, Oregon. *Contributions to Mineralogy and Petrology* **98**, 224–256.
- Bargar, K. E. & Beeson, M. H. (1985). *Hydrothermal alteration in research drill hole Y-3, Lower Geyser Basin, Yellowstone National Park, Wyoming*. US Geological Survey, Professional Paper **1054-C**.
- Beeson, M. H. & Bargar, K. E. (1984). *Major and trace element analyses of drill cores from thermal areas in Yellowstone National Park, Wyoming*. US Geological Survey, Open-File Report **84-373**.
- Bindeman, I. (2008). Oxygen isotopes in mantle and crustal magmas as revealed by single crystal analysis. In: Putirka, K. D. & Tepley, F. J., III (eds) *Minerals, Inclusions, and Volcanic Processes*. Mineralogical Society of America and Geochemical Society, *Reviews in Mineralogy and Geochemistry* **69**, 445–478.

- Bindeman, I. N. & Simakin, A. G. (2014). Rhyolites—Hard to produce, but easy to recycle and sequester: Integrating microgeochemical observations and numerical models. *Geosphere* **10**, 5.
- Bindeman, I. N., Valley, J. W., Wooden, J. L. & Persing, H. M. (2001). Post-caldera volcanism: *in situ* measurement of U–Pb age and oxygen isotope ratio in Pleistocene zircons from Yellowstone caldera. *Earth and Planetary Science Letters* **189**, 197–206.
- Bindeman, I. N., Watts, K. E., Schmitt, A. K., Morgan, L. A. & Shanks, P. W. C. (2007). Voluminous low $\delta^{18}\text{O}$ magmas in the late Miocene Heise Volcanic Field, Idaho: implications for the fate of Yellowstone hotspot calderas. *Geology* **35**, 1019–1022.
- Bohrson, W. A. & Spera, F. J. (2001). Energy-constrained open-system magmatic processes II: Application of energy-constrained assimilation–fractional crystallisation (EC-AFC) model to magmatic systems. *Journal of Petrology* **42**, 1019–1041.
- Bolte, T., Holtz, F., Almeev, R. & Nash, B. P. (2015). The Blacktail Creek Tuff: an analytical and experimental study of rhyolites from the Heise volcanic field, Yellowstone hotspot system. *Contributions to Mineralogy and Petrology* **169**, 1–24.
- Bonnichsen, B., Leeman, W. P., Honjo, N., McIntosh, W. C. & Godchaux, M. M. (2008). Miocene silicic volcanism in southwestern Idaho: geochronology, geochemistry, and evolution of the central Snake River Plain. *Bulletin of Volcanology* **70**, 315–342.
- Boroughs, S., Wolff, J. A., Bonnichsen, B., Ellis, B. S. & Larson, P. (2012). Evaluating models of the origin of Miocene low- $\delta^{18}\text{O}$ rhyolites of the Yellowstone/Columbia River large igneous province. *Earth and Planetary Science Letters* **313–314**, 45–55.
- Bowring, J. F., McLean, N. M. & Bowring, S. A. (2011). Engineering cyber infrastructure for U–Pb geochronology: Tripoli and U–Pb_Redux. *Geochemistry, Geophysics, Geosystems* **12**, Q0AA19.
- Branney, M. J. & Kokelaar, B. P. (eds) (2002). *Pyroclastic Density Currents and the Sedimentation of Ignimbrites*. Geological Society, London, *Memoirs* **27**, 152 pp.
- Branney, M. J., Bonnichsen, B., Andrews, G. D. M., Ellis, B., Barry, T. L. & McCurry, M. (2008). ‘Snake River (SR)-type’ volcanism at the Yellowstone hotspot track: distinctive products from unusual, high-temperature silicic super-eruptions. *Bulletin of Volcanology* **70**, 293–314.
- Brophy, J. (1991). Composition gaps, critical crystallinity, and fractional crystallisation in orogenic (calcalkaline) magmatic systems. *Contributions to Mineralogy and Petrology* **109**, 173–182.
- Browne, P. R. L. (1978). Hydrothermal alteration in active geothermal fields. *Annual Review of Earth and Planetary Sciences* **6**, 229–250.
- Brueseke, M. E., Hart, W. K. & Heizler, M. T. (2008). Diverse mid-Miocene silicic volcanism associated with the Yellowstone–Newberry thermal anomaly. *Bulletin of Volcanology* **70**, 343–360.
- Camp, V. E. & Ross, M. E. (2004). Mantle dynamics and genesis of mafic magmatism in the intermontane Pacific Northwest. *Journal of Geophysical Research* **109**, B08204.
- Cashman, K. V. & Giordano, G. (2014). Calderas and magma reservoirs. *Journal of Volcanology and Geothermal Research* **288**, 28–45.
- Cathey, H. E. & Nash, B. P. (2004). The Cougar Point Tuff: implications for thermochemical zonation and longevity of high-temperature, large-volume silicic magmas of the Miocene Yellowstone hotspot. *Journal of Petrology* **45**, 27–58.
- Chayes, F. (1963). Relative abundance of intermediate members of the oceanic basalt–trachyte association. *Journal of Geophysical Research* **68**, 1519–1534.
- Christiansen, E. H. & McCurry, M. (2008). Contrasting origins of Cenozoic silicic volcanic rocks from the western Cordillera of the United States. *Bulletin of Volcanology* **70**, 251–267.
- Christiansen, R. L. (2001). *The Quaternary and Pliocene Yellowstone Plateau Volcanic Field of Wyoming, Idaho, and Montana*. US Geological Survey, *Professional Papers* **729-G**, 145 pp.
- Coble, M. A. & Mahood, G. A. (2012). Initial impingement of the Yellowstone plume located by widespread silicic volcanism contemporaneous with Columbia River flood basalts. *Geology* **40**, 655–658.
- Coleman, D. S., Gray, W. & Glazner, A. F. (2004). Rethinking the emplacement and evolution of zoned plutons: Geochronologic evidence for incremental assembly of the Tuolumne Intrusive Suite, California. *Geology* **32**, 433–436.
- Colon, D. P., Bindeman, I. N., Ellis, B. S., Schmitt, A. K. & Fisher, C. M. (2015). Hydrothermal alteration and melting of the crust during the Columbia River Basalt–Snake River Plain transition and the origin of low- $\delta^{18}\text{O}$ rhyolites of the central Snake River Plain. *Lithos* **224–225**, 310–323.
- Condon, D. J., Schoene, B., McLean, N. M., Bowring, S. A. & Parrish, R. R. (2015). Metrology and traceability of U–Pb isotope dilution geochronology (EARTHTIME tracer calibration Part I). *Geochimica et Cosmochimica Acta* **164**, 464–480.
- Cooper, G. F., Wilson, C. J. N., Millet, M.-A., Baker, J. A. & Smith, E. G. C. (2012). Systematic tapping of independent magma chambers during the 1 Ma Kidnappers supereruption. *Earth and Planetary Science Letters* **313–314**, 23–33.
- DePaolo, D. (1981). Trace element and isotopic effects of combined wallrock assimilation and fractional crystallisation. *Earth and Planetary Science Letters* **53**, 189–202.
- Donoghue, E., Troll, V. R. & Harris, C. (2010). Fluid–rock interaction in the Miocene, post-caldera, Tejada Intrusive Complex, Gran Canaria (Canary Islands): insights from mineralogy, and O- and H-isotope geochemistry. *Journal of Petrology* **51**, 2149–2176.
- Drew, D. L., Bindeman, I. N., Watts, K. E., Schmitt, A. K., Fu, B. & McCurry, M. (2013). Crustal-scale recycling in caldera complexes and rift zones along the Yellowstone hotspot track: O and Hf isotopic evidence in diverse zircons from voluminous rhyolites of the Picabo volcanic field, Idaho. *Earth and Planetary Science Letters* **381**, 63–77.
- Dufek, J. & Bergantz, G. W. (2005). Lower crustal magma genesis and preservation: a stochastic framework for the evaluation of basalt–crust interaction. *Journal of Petrology* **46**, 2167–2195.
- Ellis, B. S. & Wolff, J. A. (2012). Complex storage of rhyolite in the central Snake River Plain. *Journal of Volcanology and Geothermal Research* **211**, 1–11.
- Ellis, B. S., Barry, T. L., Branney, M. J., Wolff, J. A., Bindeman, I. N., Wilson, R. & Bonnichsen, B. (2010). Petrologic constraints on the development of a large-volume, high temperature, silicic magma system: the Twin Falls eruptive centre, central Snake River Plain. *Lithos* **120**, 475–489.
- Ellis, B. S., Wolff, J. A., Boroughs, S., Mark, D., Starkel, W. & Bonnichsen, B. (2013). Rhyolitic volcanism of the central Snake River Plain: a review. *Bulletin of Volcanology* **75**, 1–19.
- Ellis, B. S., Bachmann, O. & Wolff, J. A. (2014). Cumulate fragments in silicic ignimbrites: The case of the Snake River Plain. *Geology* **42**, 431–434.
- Embree, G. F., Lovell, M. D. & Doherty, D. J. (1978). *Drilling data from Sugar City exploration well, Madison County, Idaho*. US Geological Survey Open File Report **78-1095**.
- Engleman, B., Atkinson, T., Thornton, V., Doherty, D., Moore, D., Embree, G. & Tracy, R. (2013). *Geologic Map of Ririe*

- Reservoir, Ririe, Idaho. Idaho Geological Survey, Technical Report* **13-12**.
- Friedman, I., Lipman, P. W., Obradovich, J. D., Gleason, J. D. & Christiansen, R. L. (1974). Meteoric water in magmas. *Science* **184**, 1069–1072.
- Geist, D. & Richards, M. (1993). Origin of the Columbia Plateau and Snake River plain: Deflection of the Yellowstone plume. *Geology* **21**, 789–792.
- Gelman, S. E., Gutiérrez, F. J. & Bachmann, O. (2013). On the longevity of large upper crustal silicic magma reservoirs. *Geology* **41**, 759–762.
- Gualda, G. A., Ghiorso, M. S., Lemons, R. V. & Carley, T. L. (2012). Rhyolite-MELTS: a modified calibration of MELTS optimized for silica-rich, fluid-bearing magmatic systems. *Journal of Petrology* **53**, 875–890.
- Guillong, M., Meier, D., Allan, M., Heinrich, C. & Yardley, B. (2008). SILLS: a MATLAB-based program for the reduction of laser ablation ICP-MS data of homogeneous materials and inclusions. In: Sylvester, P. (ed.) *Laser Ablation ICP-MS in the Earth Sciences: Current Practices and Outstanding Issues. Mineralogical Association of Canada, Short Course Series*. Vancouver, pp. 328–333.
- Harris, C. & Ashwal, L. D. (2002). The origin of low $\delta^{18}\text{O}$ granites and related rocks from the Seychelles. *Contributions to Mineralogy and Petrology* **143**, 366–376.
- Henshaw, N. D. (2002). Temperature of silicic magmas from the Yellowstone hotspot. MS thesis, University of Utah, Salt Lake City, 181 pp.
- Hiess, J., Condon, D. J., McLean, N. M. & Noble, S. R. (2012). $^{238}\text{U}/^{235}\text{U}$ systematics in terrestrial uranium-bearing minerals. *Science* **335**, 1610–1614.
- Hildreth, W. (1981). Gradients in silicic magma chambers: implications for lithospheric magmatism. *Journal of Geophysical Research* **86**, 10153–10192.
- Hildreth, W. (2004). Volcanological perspectives on Long Valley, Mammoth Mountain, and Mono Craters: several contiguous but discrete systems. *Journal of Volcanology and Geothermal Research* **136**, 169–198.
- Hildreth, W. & Wilson, C. J. N. (2007). Compositional zoning of the Bishop Tuff. *Journal of Petrology* **48**, 951–999.
- Hildreth, W., Christiansen, R. L. & O'Neil, J. R. (1984). Catastrophic isotopic modification of rhyolitic magma at times of caldera subsidence, Yellowstone Plateau Volcanic Field. *Journal of Geophysical Research* **89**, 8339.
- Hildreth, W., Halliday, A. N. & Christiansen, R. L. (1991). Isotopic and chemical evidence concerning the genesis and contamination of basaltic and rhyolitic magma beneath the Yellowstone Plateau Volcanic Field. *Journal of Petrology* **32**, 63–138.
- Honjo, N., Bonnicksen, B., Leeman, W. P. & Stormer, J. C. (1992). Mineralogy and geothermometry of high-temperature rhyolites from the central and western Snake River Plain. *Bulletin of Volcanology* **54**, 220–237.
- Hooper, P. R., Camp, V. E., Reidel, S. P. & Ross, M. E. (2007). The origin of the Columbia River flood basalt province: Plume versus nonplume models. In: Foulger, G. R. and Jurdy, D. M. (eds) *Plates, plumes, and planetary processes. Geological Society of America, Special Papers*, pp. 635–668.
- Husen, S., Smith, R. B. & Waite, G. P. (2004). Evidence for gas and magmatic sources beneath the Yellowstone volcanic field from seismic tomographic imaging. *Journal of Volcanology and Geothermal Research* **131**, 397–410.
- Jaffey, A. H., Flynn, K. F., Glendenin, L. E., Bentley, W. C. & Essling, A. M. (1971). Precision measurement of half-lives and specific activities of ^{235}U and ^{238}U . *Physics Reviews* **C4**, 1889–1906.
- Jarosewich, E., Nelen, J. & Norberg, J. A. (1980). Reference samples for electron microprobe analysis. *Geostandards Newsletter* **4**, 43–47.
- Jochum, K. P. & Stoll, B. (2008). Reference materials for elemental and isotopic analyses by LA-(MC)-ICP-MS: Successes and outstanding needs. In: Sylvester, P. (ed.) *Laser Ablation ICP-MS in the Earth Sciences: Current Practices and Outstanding Issues. Mineralogical Association of Canada, Short Course Series*. Vancouver, pp. 147–168.
- Karakas, O. & Dufek, J. (2015). Melt evolution and residence in extending crust: Thermal modeling of the crust and crustal magmas. *Earth and Planetary Science Letters* **425**, 131–144.
- Kokelaar, B. P., Raine, P. & Branney, M. J. (2007). Incursion of a large-volume, spatter-bearing pyroclastic density current into a caldera lake: Pavey Ark ignimbrite, Scafell caldera, England. *Bulletin of Volcanology* **70**, 23–54.
- Krogh, T. E. (1973). A low contamination method for hydrothermal decomposition of zircon and extraction of U and Pb for isotopic age determination. *Geochimica et Cosmochimica Acta* **37**, 485–494.
- Lipman, P. W. (1984). The roots of the ash flow calderas in western North America: Windows into the tops of granitic batholiths. *Journal of Geophysical Research* **89**, 8801–8841.
- Lipman, P. W. (1997). Subsidence of ash-flow calderas: relation to caldera size and magma-chamber geometry. *Bulletin of Volcanology* **59**, 198–218.
- Liu, Y., Hu, Z., Zong, K., Gao, S., Xu, J. & Chen, H. (2010). Reappraisal and refinement of zircon U–Pb isotope and trace element analyses by LA-ICP-MS. *Chinese Science Bulletin* **55**, 1535–1546.
- Loewen, M. W. & Bindeman, I. N. (2016). Oxygen isotope thermometry reveals high magmatic temperatures and short residence times in Yellowstone and other hot-dry rhyolites compared to cold-wet systems. *American Mineralogist* **101**, 1222–1227.
- Lowenstern, J. B., Smith, R. B. & Hill, D. P. (2006). Monitoring super-volcanoes: geophysical and geochemical signals at Yellowstone and other large caldera systems. *Philosophical Transactions of the Royal Society of London, Series A* **364**, 2055–2072.
- Mattinson, J. M. (2005). Zircon U–Pb chemical abrasion ('CA-TIMS') method: combined annealing and multi-step partial dissolution analysis for improved precision and accuracy of zircon ages. *Chemical Geology* **200**, 47–66.
- McCurry, M. & Rodgers, D. W. (2009). Mass transfer along the Yellowstone hot spot track I: Petrologic constraints on the volume of mantle-derived magma. *Journal of Volcanology and Geothermal Research* **188**, 86–98.
- McLean, N. M., Bowring, J. F. & Bowring, S. A. (2011). An algorithm for U–Pb isotope dilution data reduction and uncertainty propagation. *Geochemistry, Geophysics, Geosystems* **12**, Q0AA18.
- McLean, N. M., Condon, D. J., Schoene, B. & Bowring, S. A. (2015). Evaluating uncertainties in the calibration of isotopic reference materials and multi-element isotopic tracers (EARTHTIME tracer calibration part II). *Geochimica et Cosmochimica Acta* **164**, 481–501.
- Miller, J. S. & Wooden, J. L. (2004). Residence, resorption and recycling of zircons in Devils Kitchen Rhyolite, Coso Volcanic Field, California. *Journal of Petrology* **45**, 2155–2170.
- Morgan, L. A. (1992). Stratigraphic relations and paleomagnetic and geochemical correlations of ignimbrites of the Heise volcanic field, eastern Snake River Plain, eastern Idaho and western Wyoming. In: Link, P. K., Kuntz, M. A., Platt, L. B., (eds) *Regional Geology of Eastern Idaho and Western*

- Wyoming: *Geological Society of America Memoir* **179**, 215–226.
- Morgan, L. A. & McIntosh, W. C. (2005). Timing and development of the Heise volcanic field, Snake River Plain, Idaho, western USA. *Geological Society of America Bulletin* **117**, 288–306.
- Morgan, L. A., Doherty, D. J. & Leeman, W. P. (1984). Ignimbrites of the eastern Snake River Plain: Evidence for major caldera-forming eruptions. *Journal of Geophysical Research* **89**, 8665–8678.
- Nash, B. P., Perkins, M. E., Christensen, J. N., Lee, D.-C. & Halliday, A. N. (2006). The Yellowstone hotspot in space and time: Nd and Hf isotopes in silicic magmas. *Earth and Planetary Science Letters* **247**, 143–156.
- Paces, J. B. & Miller, J. D. (1993). Precise U–Pb ages of Duluth complex and related mafic intrusions, northeastern Minnesota: Geochronological insights to physical, petrogenetic, paleomagnetic, and tectonomagmatic processes associated with the 1.1 Ga midcontinent rift system. *Journal of Geophysical Research: Solid Earth (1978–2012)* **98**, 13997–14013.
- Peng, X. & Humphreys, E. D. (1998). Crustal velocity structure across the eastern Snake River Plain and the Yellowstone swell. *Journal of Geophysical Research* **103**, 7171–7186.
- Perkins, M. E. & Nash, B. P. (2002). Explosive silicic volcanism of the Yellowstone hotspot: the ash fall tuff record. *Geological Society of America Bulletin* **114**, 367–381.
- Perkins, M. E., Nash, W. P., Brown, F. H. & Fleck, R. J. (1995). Fallout tuffs of Trapper Creek Idaho—a record of Miocene explosive volcanism in the Snake River Plain volcanic province. *Geological Society of America Bulletin* **107**, 1484–1506.
- Phillips, W. M., Moore, D. K., Feeney, D. M. & Embree, G. F. (2016). Geologic map of the Heise quadrangle, Bonneville, Jefferson, and Madison counties, Idaho. *Idaho Geological Survey Digital Web Map* **176**, scale 1:24,000.
- Pierce, K. L. & Morgan, L. A. (1992). The track of the Yellowstone hotspot: volcanism, faulting, and uplift. In: Link, P. K., Kuntz, M. A. & Platt, L. B. (eds) *Regional Geology of Eastern Idaho and Western Wyoming*. *Geological Society of America, Memoirs* **179**, 1–53.
- Putirka, K. D. (2008). Thermometers and barometers for volcanic systems. In: Putirka, K. D. & Tepley, F. J., III (eds) *Minerals, Inclusions, and Volcanic Processes*. *Mineralogical Society of America and Geochemical Society, Reviews in Mineralogy and Geochemistry* **69**, 61–120.
- Riley, T. R., Leat, P. T., Pankhurst, R. J. & Harris, C. (2001). Origins of large volume rhyolitic volcanism in the Antarctic Peninsula and Patagonia by crustal melting. *Journal of Petrology* **42**, 1043–1065.
- Rowe, M. C., Ellis, B. S. & Lindeberg, A. (2012). Quantifying crystallisation and devitrification of rhyolites by means of X-ray diffraction and electron microprobe analysis. *American Mineralogist* **97**, 1685–1699.
- Schmitt, A. K., Grove, M., Harrison, T. M., Lovera, O., Hulen, J. & Walters, M. (2003). The Geysers–Cobb Mountain Magma System, California (Part 1): U–Pb zircon ages of volcanic rocks, conditions of zircon crystallisation and magma residence times. *Geochimica et Cosmochimica Acta* **67**, 3423–3442.
- Shane, P., Martin, S. B., Smith, V. C., Beggs, K. F., Darragh, M. B., Cole, J. W. & Nairn, I. A., (2007). Multiple rhyolite magmas and basalt injection in the 17.7 ka Rerewhakaaitu eruption episode from Tarawera volcanic complex, New Zealand. *Journal of Volcanology and Geothermal Research* **164**, 1–26.
- Shervais, J. W., Vetter, S. K. & Hanan, B. B. (2006). Layered mafic sill complex beneath the eastern Snake River Plain: Evidence from cyclic geochemical variations in basalt. *Geology* **34**, 365–368.
- Singer, B. S., Jicha, J. R., Condon, D. J., Macho, A. S., Hoffman, K. A., Dierkhising, J., Brown, M. C., Feinberg, J. M. & Kidane, T. (2014). Precise ages of the Réunion event and Huckleberry Ridge excursion: Episodic clustering of geomagnetic instabilities and the dynamics of flow within the outer core. *Earth and Planetary Science Letters* **405**, 25–38.
- Spray, J. G. (1997). Superfaults. *Geology* **25**, 579–582.
- Stelten, M. E., Cooper, K. M., Vazquez, J. A., Reid, M. R., Barford, G. H., Wimpenny, J. & Yin, Q.-z. (2013). Magma mixing and the generation of isotopically juvenile silicic magma at Yellowstone caldera inferred from coupling ^{238}U – ^{230}Th ages with trace elements and Hf and O isotopes in zircon and Pb isotopes in sanidine. *Contributions to Mineralogy and Petrology* **166**, 587–613.
- Sturchio, N. C., Muehlenbachs, K. & Seitz, M. G. (1986). Element redistribution during hydrothermal alteration of rhyolite in an active geothermal system: Yellowstone drill cores Y-7 and Y-8. *Geochimica et Cosmochimica Acta* **50**, 1619–1631.
- Sturchio, N. C., Keith, T. E. C. & Muehlenbachs, K. (1990). Oxygen and carbon isotope ratios of hydrothermal minerals from Yellowstone drill cores. *Journal of Volcanology and Geothermal Research* **40**, 23–37.
- Szymanowski, D., Ellis, B. S., Bachmann, O., Guillong, M. & Phillips, W. M. (2015). Bridging basalts and rhyolites in the Yellowstone–Snake River Plain volcanic province: The elusive intermediate step. *Earth and Planetary Science Letters* **415**, 80–89.
- Szymanowski, D., Ellis, B. S., Wotzlav, J. F., Buret, Y., von Quadt, A., Peytcheva, I., Bindeman, I. N. & Bachmann, O. (2016). Geochronological and isotopic records of crustal storage and assimilation in the Wolverine Creek–Conant Creek system, Heise eruptive centre, Snake River Plain. *Contributions to Mineralogy and Petrology* **171**, 106.
- Taylor, H. P. (1968). The oxygen isotope geochemistry of igneous rocks. *Contributions to Mineralogy and Petrology* **19**, 1–71.
- Taylor, H. P. (1977). Water/rock interactions and the origin of H_2O in granitic batholiths. *Journal of the Geological Society, London* **133**, 509–558.
- Vazquez, J. A., Kyriazis, S. F., Reid, M. R., Sehler, R. C. & Ramos, F. C. (2009). Thermochemical evolution of young rhyolites at Yellowstone: Evidence for a cooling but periodically replenished postcaldera magma reservoir. *Journal of Volcanology and Geothermal Research* **188**, 186–196.
- Waters, L. E. & Lange, R. A. (2015). An updated calibration of the plagioclase–liquid hygrometer–thermometer applicable to basalts through rhyolites. *American Mineralogist* **100**, 2172–2184.
- Watson, E. B. & Harrison, T. M. (1983). Zircon saturation revisited: temperature and compositional effects in a variety of crustal magma types. *Earth and Planetary Science Letters* **64**, 295–304.
- Watts, K. E., Bindeman, I. N. & Schmitt, A. K. (2011). Large-volume rhyolite genesis in caldera complexes of the Snake River Plain: insights from the Kilgore Tuff of the Heise Volcanic Field, Idaho, with comparison to Yellowstone and Bruneau–Jarbridge rhyolites. *Journal of Petrology* **52**, 857–890.
- Watts, K. E., Bindeman, I. N. & Schmitt, A. K. (2012). Crystal scale anatomy of a dying supervolcano: an isotope and geochronology study of individual phenocrysts from voluminous rhyolites of the Yellowstone caldera. *Contributions to Mineralogy and Petrology* **164**, 45–67.
- Wiesmaier, S., Troll, V. R., Carracedo, J. C., Ellam, R. M., Bindeman, I. & Wolff, J. A. (2012). Bimodality of lavas in the Teide–Pico Viejo succession in Tenerife—the role of crustal

- melting in the origin of recent phonolites. *Journal of Petrology* **53**, 2465–2495.
- Wolff, J. A., Ramos, F., Hart, G., Patterson, J. & Brandon, A. (2008). Columbia River flood basalts from a centralized crustal magmatic system. *Nature Geoscience* **1**, 177–180.
- Wolff, J. A., Ellis, B. S., Ramos, F. C., Starkel, W. A., Boroughs, S., Olin, P. H. & Bachmann, O. (2015). Remelting of cumulates as a process for producing chemical zoning in silicic tuffs: a comparison of cool, wet and hot, dry rhyolitic magma systems. *Lithos* **236–237**, 275–286.
- Wotzlaw, J.-F., Bindeman, I. N., Watts, K. E., Schmitt, A. K., Caricchi, L. & Schaltegger, U. (2014). Linking rapid magma reservoir assembly and eruption trigger mechanisms at evolved Yellowstone-type supervolcanoes. *Geology* **42**, 807–810.
- Wotzlaw, J.-F., Bindeman, I. N., Stern, R. A., D'Abzac F.-X. & Schaltegger, U. (2015). Rapid heterogeneous assembly of multiple magma reservoirs prior to Yellowstone supereruptions. *Scientific Reports* **5**, 14026.
- Yuan, H. & Dueker, K. (2005). P wave tomogram of the Yellowstone plume. *Geophysical Research Letters* **32**, L07304.